Biogeosciences

Hydrothermal trace metal release and microbial metabolism in the northeastern Lau Basin of the South Pacific Ocean

Natalie R. Cohen[1,2], Abigail E. Noble[1], Dawn M. Moran[1], Matthew R. McIlvin[1], Tyler J. Goepfert[1,3], Nicholas J. Hawco[4], Christopher R. German[1], Tristan J. Horner[1], Carl H. Lamborg[5], John P. McCrow[6], Andrew E. Allen[6], and Mak A. Saito[1]

[1]Marine Chemistry & Geochemistry Department, Woods Hole Oceanographic Institution, Woods Hole, MA 02543, USA
[2]Department of Marine Sciences, Skidaway Institute of Oceanography, University of Georgia, Savannah, GA 31411, USA
[3]School of Earth & Space Exploration, Arizona State University, Tempe, AZ 85281, USA
[4]Department of Oceanography, University of Hawai'i at Mānoa, Honolulu, HI 96822, USA
[5]Ocean Sciences Department, University of California, Santa Cruz, Santa Cruz, CA 95064, USA
[6]J. Craig Venter Institute, La Jolla, CA 92037, USA

Correspondence: Natalie R. Cohen (cohen@uga.edu) and Mak A. Saito (msaito@whoi.edu)

Abstract. Bioactive trace metals are critical micronutrients for marine microorganisms due to their role in mediating biological redox reactions, and complex biogeochemical processes control their distributions. Hydrothermal vents may represent an important source of metals to microorganisms, especially those inhabiting low-iron waters, such as in the southwest Pacific Ocean. Previous measurements of primordial ^{3}He indicate a significant hydrothermal source originating in the northeastern (NE) Lau Basin, with the plume advecting into the southwest Pacific Ocean at 1500–2000 m depth (Lupton et al., 2004). Studies investigating the long-range transport of trace metals associated with such dispersing plumes are rare, and the biogeochemical impacts on local microbial physiology have not yet been described. Here we quantified dissolved metals and assessed microbial metaproteomes across a transect spanning the tropical and equatorial Pacific with a focus on the hydrothermally active NE Lau Basin and report elevated iron and manganese concentrations across 441 km of the southwest Pacific. The most intense signal was detected near the Mangatolo Triple Junction (MTJ) and Northeast Lau Spreading Center (NELSC), in close proximity to the previously reported ^{3}He signature. Protein content in distal-plume-influenced seawater, which was high in metals, was overall similar to background locations, though key prokaryotic proteins involved in metal and organic uptake, protein degradation, and chemoautotrophy were abundant compared to deep waters outside of the distal plume. Our results demonstrate that trace metals derived from the NE Lau Basin are transported over appreciable distances into the southwest Pacific Ocean and that bioactive chemical resources released from submarine vent systems are utilized by surrounding deep-sea microbes, influencing both their physiology and their contributions to ocean biogeochemical cycling.

1 Introduction

The central Pacific Ocean encompasses several biogeochemical regimes, including low-nitrate surface waters in the subtropical gyres and high-nitrate, yet low-iron waters in the equatorial upwelling zone (Cohen et al., 2021a; Moore et al., 2013, 2001; Saito et al., 2014). Towards the South Pacific Ocean, little dust input from continental sources combined with low macronutrient concentrations results in low primary productivity and reduced biological carbon export to the deep ocean (Jickells et al., 2005). In this region, active hydrothermal venting may be an important source of trace metals, such as iron, to surrounding microorganisms.

Hydrothermal venting can arise wherever seawater percolating down into the seafloor intercepts strong geothermal gradients, for example as imposed by magmatic activ-

ity in the upper ocean crust. Such systems can be associated with mid-ocean ridge spreading centers, intra-plate volcanoes, convergent margins, subduction zones, island arc volcanoes, and back-arc spreading centers (Beaulieu et al., 2013; German and Seyfried, 2013). High-temperature fluids released from vents serve as sources of dissolved elements by enriching seawater in metals derived from the underlying crust. The chemicals most concentrated in vent fluids include iron (Fe), manganese (Mn), zinc (Zn), copper (Cu), methane, and sulfides. They reach millimolar to micromolar concentrations compared to the picomolar to nanomolar range typical of background seawater and are used as energy sources for chemosynthetic microbial communities that sustain rich food webs (Bruland and Lohan, 2003; Tivey, 2007). A substantial portion of these hydrothermally released trace metals rapidly precipitate as mineral sulfides and oxides through abiotic and biological oxidation (Gartman and Findlay, 2020). The hydrothermal fluid mixes with cool, oxidizing seawater and rises to form buoyant plumes above vent sources. Once the buoyant plumes reach neutral density in the water column, they are spread laterally by prevailing deep-sea currents, transporting chemical resources and microbial communities into the deep ocean interior in non-buoyant plumes (Dick et al., 2013; Reed et al., 2015). Trace metal concentrations within these plumes generally decrease with distance from the hydrothermal source as a result of dilution and removal processes that include both abiotic precipitation and microbial uptake (Cowen et al., 1990; Gartman and Findlay, 2020).

However, recent observations demonstrate that detectable levels of metals such as Fe can be transported substantial distances from vent sources, with both dissolved and particulate hydrothermally sourced Fe traveling up to thousands of kilometers, tracking with primordial [3]He released from the mantle during hydrothermal venting (Fitzsimmons et al., 2014, 2017; Resing et al., 2015; Saito et al., 2013). The Fe isotopic composition of central Pacific seawater furthermore indicates that such distal transport of hydrothermal Fe has likely persisted over the Cenozoic (Horner et al., 2015). Non-buoyant plume Fe is thought to be stabilized in the dissolved state as inorganic metal oxides as well as organic and inorganic colloids and through organic ligand complexation (Bennett et al., 2008; Fitzsimmons et al., 2014, 2017; Gartman and Findlay, 2020; Hawkes et al., 2013). The next largest [3]He signal in the Pacific Ocean after the southern East Pacific Rise is associated with the Lo'ihi Seamount system, which similarly produces a strong distal Fe plume (Jenkins et al., 2020). It remains to be determined whether trace metals are similarly advected from the northeastern (NE) Lau Basin, where the third-largest hydrothermal [3]He signal in the Pacific Ocean has been measured, extending 2000 km to the northwest and representing the most intense hydrothermal signature in this ocean basin at ∼ 1700 m depth (German et al., 2006; Lupton et al., 2004).

The NE Lau Basin is a dynamic back-arc spreading region surrounded by plate boundaries in the tropical southwest Pacific that contains an abundance of hydrothermal vent fields (Baker et al., 2019; Beaulieu et al., 2013; Martinez et al., 2006). The basin is topographically restricted by the Lau and Tonga ridges, which converge to the south (Speer and Thurnherr, 2012). Consequently, deep hydrothermal plumes can only escape the Lau Basin from the north, exiting into the southwest Pacific (German et al., 2006; Speer and Thurnherr, 2012). The contributions of the prominent hydrothermal plume located off the Tonga Ridge (15° S and 173.1° W) to metal biogeochemistry and microbial physiology have yet to be investigated. In addition to its unique geophysical properties, the NE Lau Basin contains mineral deposits of commercial interest. The hydrothermal sulfides from this region contain the highest gold contents on record (Herzig et al., 1993), and plans are ongoing to mine cobalt- and nickel-rich ferromanganese nodules from the seafloor to meet increasing economic demands (Lusty and Murton, 2018).

Recent studies suggest that in addition to distal hydrothermal plumes introducing a flux of chemically reduced elements and compounds to the ocean interior, these systems may impact metal availability to surface phytoplankton. The oligotrophic South Pacific has extraordinarily low levels of continentally derived Fe and low macronutrient concentrations, resulting in nitrate and Fe limitation of phytoplankton growth (Jickells et al., 2005; Sunda, 2012; Behrenfeld et al., 2006). Hydrothermally sourced, distally transported Fe from the southern East Pacific Rise and Lo'ihi distal-plume systems may eventually upwell to fertilize surface phytoplankton communities in the Southern Ocean and the subpolar North Pacific, respectively (Jenkins et al., 2020; Resing et al., 2015). Distally transported Fe from the NE Lau Basin is therefore not only critical to consider in the aphotic ocean; it could contribute euphotic zone primary production depending on water mass circulation and upwelling dynamics (Jenkins et al., 2020; Tagliabue et al., 2010).

Trace metal transformations in hydrothermal plumes are heavily driven by biological communities (Gartman and Findlay, 2020; Toner et al., 2009, 2016). Prior microbiological and meta-omic studies have offered insights into plume microbial community dynamics, with many studies focusing on near-field ecosystems (Huber et al., 2007; Jeanthon, 2000; Li et al., 2014; Reveillaud et al., 2016; Sylvan et al., 2012; Takai et al., 2008) and fewer, more recent explorations into distal plumes (Djurhuus et al., 2017; Haalboom et al., 2020; Li et al., 2020). Microbial communities in plumes may be sourced from seafloor vent sites themselves or seeded from background seawater (Dick et al., 2013; Reed et al., 2015; Sheik et al., 2015). They include members of the Gammaproteobacteria, Thaumarchaea, and Deltaproteobacteria (Anantharaman et al., 2016; Dick et al., 2013), with these groups decreasing with distance from the vent source (Haalboom et al., 2020). Chemosynthetic bacteria in hydrothermal plumes carry out sulfur, methane, ammonia, hydrogen, and Mn oxi-

dation, sharing functional characteristics with microbes from other reducing habitats (Anantharaman et al., 2016; Dick et al., 2013). The less frequently studied hydrothermal microeukaryote populations include Archaeplastida, ciliates, dinoflagellates, Rhizaria, stramenopiles, and fungi, which have been identified based on partial metagenome-assembled genomes and amplicon sequencing (Anantharaman et al., 2016; Hu et al., 2021), and play an important role in plume organic carbon cycling via grazing (Bennett et al., 2013; Hu et al., 2021). Microbial community dynamics, ecology, and biogeochemical contributions are comparatively less studied in distal hydrothermal plumes due to their more recent characterization and fewer interdisciplinary expeditions where both the geochemistry and microbiology of ecosystems are considered.

The 2011 MetZyme expedition embarked across the central Pacific Ocean with the goal of connecting trace element distributions with protein metabolism, and a suite of biological and physiochemical parameters were collected along vertical and lateral ocean gradients (Cohen et al., 2021a; Hawco et al., 2020; Munson et al., 2015; Saito et al., 2014, 2015, 2020; Santoro et al., 2017). The trace metal profiles across this section of the Pacific Ocean and the sources and sinks driving their distributions have not yet been described. In this study, we present the full-depth dissolved trace metal section to address whether hydrothermal activity previously measured in the northeastern edge of the Lau Basin is associated with trace metal input, and we leverage the MetZyme protein data set to determine whether surrounding microbes were sensitive to distal hydrothermal-plume geochemistry. Our results indicate several hydrothermal features based on dissolved Fe and Mn profile anomalies, with relatively abundant proteins related to protein folding, protease activity, and metal transport in the vicinity of a hydrothermal plume. We posit that these hydrothermal sources are a significant contributor to metal biogeochemistry and microbial physiology in the tropical southwest Pacific Ocean.

2 Methods

2.1 Oceanographic sampling section and biomass collection

Seawater sampling occurred from 1–25 October 2011 on board the R/V *Kilo Moana* during the MetZyme expedition (Saito et al., 2014). The meridional transect (17° N–15° S) began off the Hawaiian Islands and terminated in the Tonga–Fiji region (173.1° W) of the NE Lau Basin (Fig. 1). Biomass collection for metaproteomics was performed using battery-operated underwater McLane pumps (McLane Research Laboratories) outfitted with custom filter head units secured onto a trace metal clean winch line. Each McLane pump head had three filter fractions for targeting specific size classes of the microbial community. For this analy-

sis, we considered the 3–51 µm fraction containing eukaryotic protists and particle-associated and/or adsorbed bacteria, archaea, and viruses. Pumps filtered between ∼ 100–1000 L and once retrieved on board were promptly sectioned for omic analyses (16S/18S rRNA, proteins) and frozen at −80 °C (Table S1). Meta-omics was performed across lateral and vertical gradients of the transect (Cohen et al., 2021a).

2.2 Trace metal analyses

Seawater samples for trace metal analyses were collected using a trace metal clean rosette consisting of 12 ∼ 8 L X-Niskins on a trace metal clean AmSteel winch line (Saito et al., 2014). Two sets of 12 Niskin bottles were used for full stations to allow simultaneous casting and processing. Following seawater collection, X-Niskins were brought into a fabricated shipboard class 100 clean room and pressurized with filtered high-purity nitrogen gas. Seawater was filtered through 47 mm 0.2 µm polyethersulfone (Pall Supor) membranes to remove the particulate fraction, which was saved for the particulate metal analysis. The filters were not rinsed with Milli-Q water prior to freezing. HEPA filters were used to minimize particle contamination, and trace metal clean approaches were used during filtration and sample handling procedures. Prior to sample collection, polyethylene bottles were cleaned by soaking for 2 weeks in 10 % HCl (Baker Analyzed ACS reagent) and by rinsing with pH 2 HCl. Seawater was acidified to pH 1.8 using hydrochloric acid (Optima grade, Fisher Chemical), and samples were stored for 8 years before this dissolved trace metal analysis was conducted.

Seawater preconcentration was performed using an automated solid-phase extraction system, seaFAST pico, run in offline concentration mode (Bown et al., 2017; Jackson et al., 2018; Rapp et al., 2017; Wilson et al., 2019; Wuttig et al., 2019). The seaFAST contains a Nobias-chelate PA1 resin column (ethylenediaminetriacetate and iminodiacetate) suitable for the simultaneous preconcentration of several trace metals (Fe, Mn, Zn, Cu, Cd, Ni) with high sensitivity and quantitative recovery (Biller and Bruland, 2012; Sohrin et al., 2008). Reagents consisted of a 4 M ammonium acetate pH 6.0 buffer (Elemental Scientific), a 1 % nitric acid rinse solution (Optima grade, Fisher Chemical), 10 % nitric acid elution acid (Optima grade, Fisher Chemical), and a second "internal standard" 10 % nitric elution acid solution containing 10 ppb indium ([115]In; SPEX CertiPrep). Solutions were prepared with 18.2Ω Milli-Q water (Millipore). Polypropylene conical tubes used in the autosampler were HCl-acid-soaked for 1 week and pH 2-rinsed prior to use. Acidified samples were preconcentrated using an initial volume of 30–33 mL and elution volume of 500 µL. The volume range is due to early samples being run with four 10 mL loop load cycles (exactly 40 mL seawater as the initial volume). The seaFAST vacuum overflows the load loop, which resulted in only ∼ 3 mL remaining during the last 10 mL cycle and a resulting concentration factor of approximately 66. All sub-

sequent samples were run with three full 10 mL load cycles for a concentration factor of 60. Process blanks consisted of Milli-Q HCl-acidified to pH 2 (Optima grade, Fisher Chemical) and were run alongside samples to account for background reagent and sample handling contamination.

Following offline seaFAST preconcentration, the multi-element quantitative analysis was performed using an iCAP Q inductively coupled plasma mass spectrometer (ICP-MS; Thermo Scientific) with a quartz cyclonic spray chamber (Thermo Scientific). Oxide interference on metal isotopes was minimized through the use of a cooled spray chamber and helium collision gas. Analytes were measured in single quadruple mode (kinetic energy discrimination, KED). Concentrations of Fe, Mn, Zn, Cu, and Cd were determined using a six-point external standard curve with a multi-element standard (SPEX CertiPrep), diluted to range from 1–10 ppb in 5 % nitric acid and prepared using volumetric flasks. Indium (In) standards (SPEX CertiPrep) were similarly added to these standard stocks, diluted to 1, 2, 3, 4, and 10 ppb. Instrument injection blanks consisted of 5 % nitric acid in Milli-Q. Standard curve R^2 values were ≥ 0.98 for the elements monitored.

Using this resin-based preconcentration method, recoveries have been demonstrated to be $> 98\%$ (Biller and Bruland 2012). In this analysis, matrix corrections were calculated using the known amount of In added to elution acid (10 ppb) and In counts per second (cps) values measured in each eluted sample, which averaged $83 \pm 9\%$. Since In was added in the elution acid and not to the sample prior to preconcentration, this is considered a matrix correction and not recovery efficiency. Dissolved metal concentrations (dTM; nM) were calculated for each metal following Eq. (1):

$$dTM = \frac{M_{\text{Sample}}}{In_{\text{Sample}}} - \frac{M_{\text{Process}}}{In_{\text{Process}}} \times \frac{In_{\text{Elution}}}{M_{\text{Slope}}} \times \frac{V_{\text{Eluted}}}{V_{\text{Original}}}, \qquad (1)$$

where M_{Sample} represents the metal cps in a given sample; In_{Sample} is the ^{115}In cps of the sample; M_{Process} and In_{Process} are the average metal and ^{115}In cps, respectively, of the pH 2 process blanks; In_{elution} is the ^{115}In cps of the solution used to elute metals off the resin column; M_{slope} is the slope (cps/ppb) of metal M determined with the SPEX standards; V_{Original} is the volume preconcentrated (30 or 33 mL); and V_{Eluted} is the final volume eluted (500 μL) for a concentration factor of 60 or 66.

Method accuracy and precision were assessed using the 2009 GEOTRACES coastal surface seawater (GSC) standard ($n = 3$; Table 1, Fig. S1), where estimated precision was 0.6 % (Fe), 7.2 % (Cu), 2.4 % (Cd), 7.4 % (Cd), and 2.1 % (Mn) relative standard deviation (RSD). We observed higher variability among standard runs for Zn likely due to handling contamination, with 25.5 % RSD. Internal consistency was achieved by running previously analyzed deep seawater (from St. 9 and St. 13) alongside samples to monitor seaFAST accuracy over time and to account for newly made batches of reagents and resin columns. Samples ap-

Table 1. Reference seawater comparisons using the 2009 GEO-TRACES coastal surface seawater (GSC) standard.

Metal	This study ($n = 3$) (nM)	GEOTRACES consensus (nM)
Fe	1.74 ± 0.01	1.56 ± 0.12
Zn	1.37 ± 0.35	1.45 ± 0.10
Cu	1.53 ± 0.11	1.12 ± 0.15
Cd	0.41 ± 0.01	0.37 ± 0.02
Ni	4.61 ± 0.34	4.5 ± 0.21
Mn	2.33 ± 0.05	2.23 ± 0.08

pearing oceanographically inconsistent with adjacent seawater depths were subsequently re-run. Comparisons of Met-Zyme profiles alongside the closest GP16 station in the South Pacific are presented in Fig. S2.

Our data showed a systematic Cu offset with concentrations that were 7 %–22 % higher than consensus values (Table 1, Fig. S1). We are unsure if this is associated with an offset in our method or with the emerging notion that Cu may be underestimated in prior consensus standard reporting. Cu speciation is known to include kinetically inert species (Kogut and Voelker, 2003), which could be resistant to exchange with preconcentration resins. It is possible that our higher dCu concentrations are a result of long-term acidified storage (8 years), during which time strongly binding refractory organic complexes could degrade and increase labile Cu (Little et al., 2018). Along these lines, Posacka et al. (2017) determined that labile Cu concentrations in non-UV-oxidized seawater samples increase with storage time, with long-term sample storage at low pH (> 4 years) demonstrating similar concentrations to those UV-oxidized and measured within 2 months. Dissolved Cu has previously been reported as 3.1 nM in the deep southwest Pacific using Nobias-chelate PA1 resin (Takano et al., 2017), whereas the maximum raw dCu concentration we obtained in the southwest Pacific was approximately 4.2 nM. It is furthermore possible that the matrix corrections based on In are not reflective of Cu, which has been demonstrated to show both high (103 %) and low ($\sim 50\%$) recoveries from Nobias resin at pH of 6.1 (Quéroué et al., 2014; Rapp et al., 2017). In addition, ArNa$^+$ interferences on ^{63}Cu cannot be completely ruled out given the abundance of Na$^+$ in seawater (Diemer et al., 2002), although a cooled spray chamber was used to minimize such polyatomic interferences. The exact mechanism behind these elevated Cu concentrations is unclear at present, and an intercalibration exercise within the trace metal community using long-term-stored seawater would be useful to further understand these offsets.

Laboratory blanks consisted of Milli-Q (MQ) acidified to a pH of 2 with Optima-grade HCl and were run alongside seawater samples (Table 2). Blanks reflect contamination added from reagents, seaFAST tubing, and laboratory and ship-

board sample handling. MQ blanks showing pronounced Fe and/or Zn contamination were removed from the data set. The detection limit (LOD) was determined using 3 times the standard deviation of the pH 2 blanks. In runs where only one MQ blank was used, the LOD could not be determined.

The seaFAST was used to quantify dissolved Fe, Mn, Zn, Cu, Ni, and Cd. To accurately quantify Co, UV oxidation is necessary to disrupt strong organic ligands associations, and irradiation was not performed on seaFAST-preconcentrated seawater samples. A substantial fraction of the total dissolved Co was strongly bound to organic ligands, unchelated by the Nobias resin, and lost during the preconcentration procedure (Saito and Moffett, 2001; Billard and Bruland, 2012; Milne et al., 2010; Ndung'u et al., 2003). Instead, dissolved-Co data are presented using cathodic stripping voltammetry with seawater exposed to UV oxidation for 1 h, as previously published by Hawco et al. (2020).

Filter fractions for the particulate metal analysis were digested in 50 % nitric acid and heated for 3 h at 90 °C, using 1 ppb In as an internal standard, diluted with 5 % nitric acid and quantified on an Element2 ICP-MS alongside external SPEX standards (Goepfert, 2013). Originally, blanks consisted of 0.2 µm polyethersulfone (Pall Supor) filters that were soaked in 10 % HCl and rinsed with MQ until a neutral pH was achieved. These filters were not rinsed with ultra-filtered seawater. Metal contamination on these filter blanks was high, with metal counts orders of magnitude lower in all filters exposed to seawater. We suspect that metals derived from the cleaning acid were retained on the filters, and seawater conditioning and flushing would have reduced this contamination. We instead calculate particulate metal (pM) concentrations using minimum pFe and pMn values largely derived from oxygen minimum zone (OMZ) depths as low metal reference "blanks", which is a conservative approach and underestimates true particulate metal concentrations. All particulate metal samples were analyzed over three ICP-MS runs, with the designated blank filters containing approximately 117–240 pM Fe and 3–12 pM Mn. The Fe blanks correspond to St. 1 400, St. 2 450, and St. 4 150 m, and the Mn blanks correspond to St. 2 225, St. 4 400, and St. 5 800 m.

2.3 Metaproteomics

Biomass was collected onto 3–51 µm filters using in situ battery-operated McLane pumps which filtered 165–1384 L of seawater over the course of several hours, with flow rate depending on the suspended load present (Table S1). Seawater was first passed through a 51 µm pre-filter to exclude multi-cellular organisms, aggregated colonies, and large organic debris followed by 3 and 0.2 µm filter membranes to capture the microeukaryotic and prokaryotic communities, respectively. Filters were frozen at −80 °C until laboratory extractions. Proteins were extracted following a sodium dodecyl sulfate (SDS) detergent-based method to solubilize membrane and soluble proteins and heated for 10 min at 95 °C (Cohen et al., 2021a; Saito et al., 2014). Protein quantification was performed using a colorimetric Bradford protein assay with the bovine serum albumin standard and a NanoDrop spectrophotometer. Digestion was performed using trypsin at a trypsin–protein ratio of 1 : 20, and peptides were further purified using C18 Ziptips. For the mass spectrometry analysis, peptides were diluted to $0.1 \, \mu g \, \mu L^{-1}$, and approximately 0.5–2 µg was injected onto a Dionex Ultimate3000 RSLCnano HPLC system in two-dimension active modulation mode coupled to a Thermo Fusion Orbitrap mass spectrometer operating in data-dependent acquisition mode (McIlvin and Saito, 2021). For St. 1 200, 300, and 400 m, $\sim 0.5 \, \mu g$ of peptides was injected due to low remaining peptide yields, whereas 2 µg was injected for all other samples. The mass spectrometer monitored MS^1 scans from 380–1580 m/z at 240 K resolution, and MS^2 scans had a 1.6 m/z isolation window, 50 ms maximum injection, and a 5 s dynamic exclusion.

A translated metatranscriptome was used as the protein database (Cohen et al., 2021a). Briefly, the metatranscriptomic data were generated by extracting RNA from 3–51 µm size fraction filters, purifying RNA, removing ribosomal RNA, converting RNA to cDNA followed by amplification, and fragmenting to 200 bp. Libraries were sequenced on the Illumina HiSeq platform, and raw data are available through the National Center for Biotechnology (NCBI) under bioproject PRJNA555787. Bioinformatic processing consisted of adaptor trimming, de novo assembly, open reading frame (ORF) prediction, and read mapping to ORFs (Cohen et al., 2021a). Taxonomic and functional annotations were performed using the custom-built database PhyloDB, which includes marine prokaryotic and eukaryotic references (https://github.com/allenlab/PhyloDB, last access: 26 September 2021), and additional iron oxidation, reduction, storage, and acquisition annotations were assigned using FeGenie (Garber et al., 2020).

Metaproteomic spectral matches were performed using the SEQUEST algorithm within Proteome Discoverer using a fragment tolerance of 0.6 Da and parent tolerance of 10 ppm. Identification criteria consisted of a peptide threshold of 95 % (one peptide minimum) and protein threshold of 99 % in Scaffold (version 4.8.4, Proteome Software Inc.). Exclusive spectral counts were normalized following the normalized spectral abundance factor (NSAF) approach, which accounts for differences in total spectral counts among samples and enables a relative comparison (Cohen et al., 2021a). ORFs with a classified taxonomic annotation and lineage probability index greater than 0.7 were used for the downstream analysis (Podell and Gaasterland, 2007). A small value of 0.03 (approximately the lowest normalized spectral count value in the data set) was added to all counts, thereby removing instances of 0, and allowed for fold change estimates. A permutation test was used to determine differential abundance of proteins between the hydrothermally influenced sample ($n = 1$) and background sites ($n = 20$) im-

Table 2. The seaFAST blanks and limits of detection determined by converting cps to nanomolar and correcting for matrix effects. MQ blank concentrations shown are averages across runs ± 1 standard deviation, with replicate blanks averaged within runs. The number of test sets (n) represents individual ICP-MS runs where blanks were preconcentrated alongside seawater samples and analyzed via ICP-MS. * For Zn, high-MQ blanks were observed in four runs, and these values were excluded from the blank averages and LOD shown.

	Fe (nM)	Mn (nM)	*Zn (nM)	Cu (nM)	Ni (nM)	Cd (nM)
LOD ($n = 12$)	0.10 ± 0.11	0.006 ± 0.007	0.65 ± 0.39	0.11 ± 0.23	0.04 ± 0.02	0.0008 ± 0.0005
MQ Blank ($n = 18$)	0.14 ± 0.10	0.006 ± 0.005	0.47 ± 0.22	0.06 ± 0.08	0.04 ± 0.03	0.0006 ± 0.0003

plemented in PANDA-view (Chang et al., 2018). *P* values were multiple-test-corrected using the Benjamini–Hochberg method, and the significance cutoff was a false discovery rate (FDR) < 0.1.

2.4 Amplicon sequencing

Taxonomic composition was further assessed using 18S and 16S ribosomal RNA (rRNA) amplicon sequencing from the 3–51 µm filter size fraction (Cohen et al., 2021a). The V3–V5 and V9 regions of the 16S and 18S rRNA fragments, respectively, were targeted and sequenced using the Roche 454 platform. The full cDNA prep and bioinformatic processing details are described in Bertrand et al. (2015). The 16S rRNA operational taxonomic units (OTUs) were taxonomically annotated using the SILVA rRNA database (release 111) (Quast et al., 2013) and 18S rRNA OTUs using the Protist Ribosomal Reference v.4.11.1 database (Guillou et al., 2013). Principal coordinate analysis (PCoA) of OTU data was performed using Bray–Curtis dissimilarity on center-log-ratio transformed values and implemented with the R package *phyloseq* (McMurdie and Holmes, 2013).

3 Results and discussion

The objective of the MetZyme survey was to track how microbial physiology shifts along natural biogeochemical gradients, with an emphasis here on the tectonically active tropical southwest Pacific (Baker et al., 2019; Beaulieu et al., 2013). The section spans multiple biomes, beginning in the oligotrophic tropical North Pacific gyre, latitudinally traversing the nutrient-rich equatorial upwelling zone, and terminating in the oligotrophic South Pacific gyre with a short longitudinal transect off the Samoan Islands, in the vicinity of the NE Lau Basin (Fig. 1).

Physiochemical measurements indicated an asymmetry between the tropical Northern Hemisphere and Southern Hemisphere with a difference in thermocline and nutricline depths, oxygen saturation, particle density (turbidity), and salinity (Fig. S3). An oxygen minimum zone (OMZ) resided between $17°$ N and $3.5°$ S at 150–1000 m depth, with the OMZ layer directly above excess nitrate + nitrite and phosphate in the northern tropical Pacific (Fig. 1). Equatorial upwelling was evident with nitrate + nitrite and phosphate con-

centrations reaching 10 and 0.5 µM, respectively, in surface waters between 0–3.5° S. Distinct water masses were observed across the section with higher-salinity surface water characteristic of the South Equatorial Pacific Intermediate Water present south of the Equator and the North Equatorial Pacific Intermediate Water to the north (Bostock et al., 2010). The South Equatorial Pacific Intermediate Water is associated with a deepening of the thermocline also evident in macronutrient and trace metal nutriclines, with on average < 0.15 nM dFe, < 0.6 nM dZn, < 0.6 nM dCu, < 3.1 nM dNi, < 80 pM dCd, and < 25 pM dCo persisting to 300 m in the South Pacific (Fig. 1). Below we report the full-depth trace metal distributions along this natural biogeochemical gradient.

3.1 Biogeochemical controls on dissolved metals in the tropical Pacific (St. 1-8)

Dissolved metal distributions in the northern transect (St. 1–8) reflected regional biogeochemical and physical influences, including biological nutrient utilization in surface waters, redox effects in oxygen minimum zones, heterotrophic remineralization, hydrothermal input, and deep-water scavenging (sorption onto particles, abiotic precipitation, aggregation of colloids, and biologically mediated precipitation; Fig. 1). Dissolved Fe showed a classic hybrid-type profile (Bruland and Lohan, 2003), with average concentrations of 0.15 ± 0.10 nM in surface waters (< 200 m) due to biological drawdown, increasing to 0.63 ± 0.30 nM below the euphotic zone as a result of remineralization (200–3000 m) and stabilizing to an average of 0.65 ± 0.14 nM across the abyssal ocean (> 3000 m; Fig. 2). In contrast to dFe, dMn was elevated in surface waters due to dust input and photoreduction (van Hulten et al., 2017; Sunda et al., 1983), reaching an average 0.80 ± 0.30 nM at 40 m and decreasing to 0.20 ± 0.03 nM by 3000 m. These Mn distributions are typical of the deep Pacific Ocean, with Mn oxidation mediated by Mn-oxidizing bacteria in aphotic waters (van Hulten et al., 2017; Moffett and Ho, 1996; Tebo et al., 2005).

A hydrothermal dFe signal was captured off the Hawaiian Island chain at St. 1 ($17°$ N, $154.4°$ W; Fig. 2), ~ 212 km away from the tectonically active Lo'ihi Seamount. Maximum dFe concentrations reached 1.26 nM at 1000 m, consistent with the 1100 m Lo'ihi injection depth and associated [3]He signature (Boyle et al., 2005; Jenkins et al., 2020; Lup-
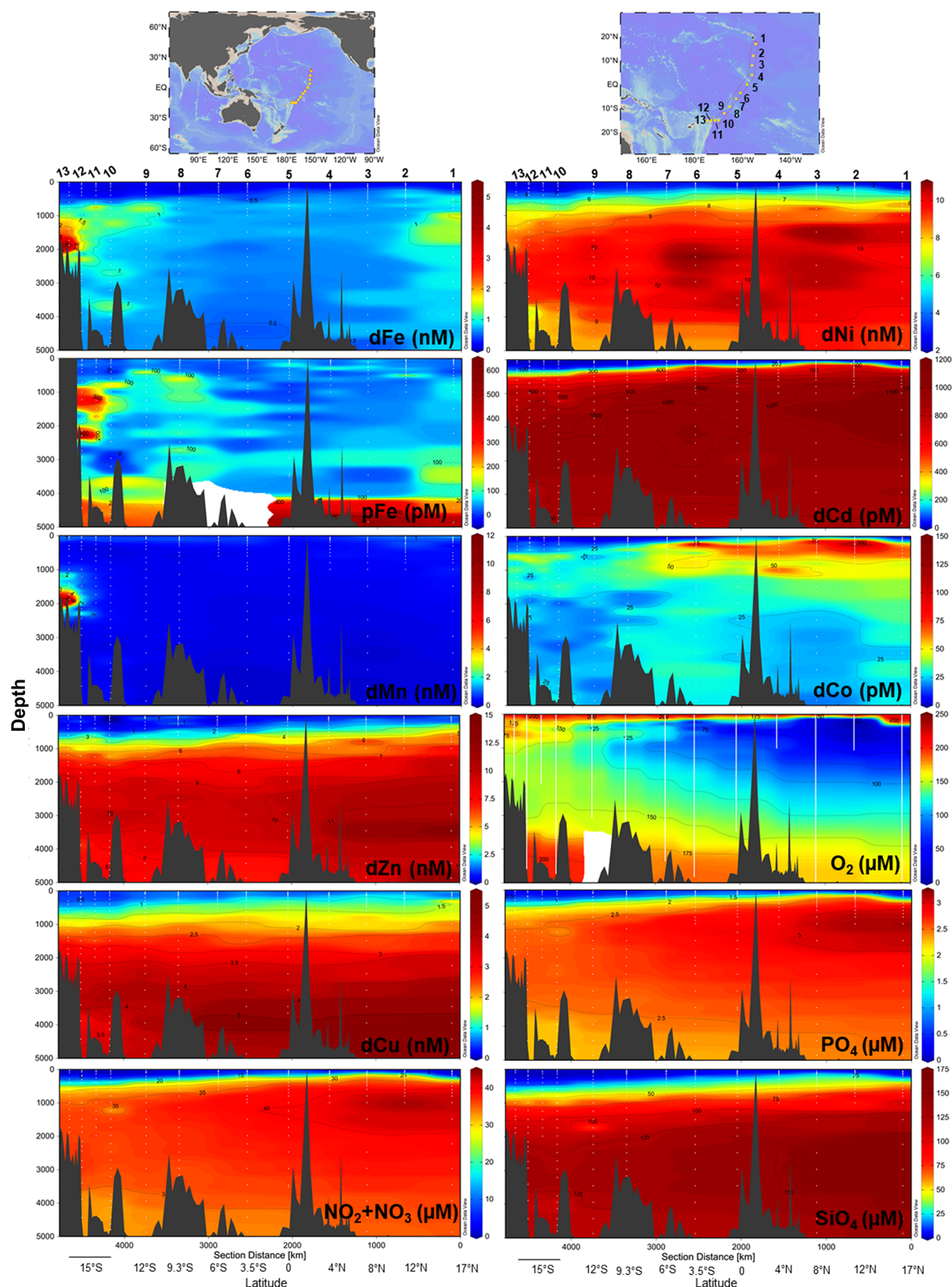
Figure 1. Trace metal and macronutrient section plots along the MetZyme transect plotted using weighted-gridding interpolation in Ocean Data View. All dissolved metals apart from Co were quantified using seaFAST ICP-MS, while Co was measured using cathodic stripping voltammetry following UV irradiation. Vertical white lines mark the CTD instrument casts; white dots indicate discrete sampling depths. Six Fe outliers were removed from the section; for full profiles see Figs. 2–4.

ton et al., 2004; Wu et al., 2011). Using historical He concentrations and isotope ratio anomalies (δ^3He) from the distal Lo'ihi plume close to our site (17° S, 152° W; Jenkins et al., 2019a) and converted to excess ^{3}He (Jenkins et al., 2019b, 2020), we calculate a dFe:^{3}He slope ratio of 2.0×10^6. This ratio is in good agreement (to within a factor of 2) with the distal ratio reported by Jenkins et al. (2020) using multiple distal sites 100–1000 km from Lo'ihi. Dissolved Mn distributions show only a minor enrichment at this depth, similar to previous observations (Boyle et al., 2005), and support high dFe:dMn ratios associated with the Lo'ihi hydrothermal system (Jenkins et al., 2020).

Dissolved Co, like Mn and Fe, reflected a hybrid-type profile with biological uptake in the euphotic zone, remineralization, and scavenging influencing its distribution (Fig. 3). In the OMZs located between St. 1–6 (Fig. 1), two dCo plumes were apparent with dCo maxima of 132 pM (St. 2; 1.7 µM O_2) and 116 pM dCo (St. 6; 26 µM O_2) centered at ∼ 200 m, as previously discussed for the MetZyme section (Hawco et al., 2020). Dissolved Co is hypothesized to accumulate in the OMZ due to decreased activity of Mn-oxidizing bacteria, which otherwise co-precipitate Co along with Mn oxides onto their cell surface under oxic conditions (Cowen and Bruland, 1985; Hawco et al., 2020; Saito et al., 2017). Although dMn shows minor enrichment at St. 2 in the OMZ, coinciding with high dCo, this biological feature appears to be secondary to surface photoreduction and deep-scavenging processes which strongly drive its vertical profile.

Other bioactive trace metals, including Zn, Cu, Ni, and Cd, by contrast followed nutrient-like distributions with biological drawdown resulting in low concentrations in surface waters and accumulation of dissolved metals at depth (Figs. 3–4). Dissolved Zn was on average 1.21 ± 1.42 nM in surface waters of 40 m and 10.37 ± 0.73 nM by 3000 m. Dissolved Zn distributions are supported by a strong linear relationship with SiO_4 along the cruise transect, with a Zn : Si slope of 0.069 nmol : µmol and an R^2 of 0.96 (Fig. 3b), which matches the tropical southeast Pacific value of 0.066 (Roshan et al., 2016). This slope furthermore is close to the 0.053 nmol : µmol ratio used to calibrate Zn : Ca proxies (Marchitto et al., 2000), which is known to deviate depending on ocean basin (Middag et al., 2019). Dissolved Cu was an average of 0.62 ± 0.12 nM in surface waters of 40 m and 4.15 ± 0.19 nM by 3000 m, while dNi showed surface concentrations of 2.54 ± 0.40 nM and 10.25 ± 0.34 nM by 3000 m.

In the case of dCd, its stoichiometry (Cd : PO_4) varied with depth and between hemispheres, likely due to biological drawdown in surface waters, remineralization at depth, and mixing of water masses. Dissolved Cd ranged from 3 to 1129 pM across the section, with an average of 9 ± 6 pM at 40 m and 979 ± 40 by bathypelagic depths of 3000 m. Cd showed multiple linear relationships with PO_4, where the Cd : PO_4 ratio reached 116 pmol : µmol in surface waters < 1 µM PO_4 and increased to 462 in deep waters containing > 1 µM PO_4 (Fig. 4b). Our ratios are consistent with reported slopes of 50 in surface waters and 410 in deep waters of the southwest Pacific (Sieber et al., 2019) and 88 in surface waters (< 250 m) and 420 in deep waters (> 250 m) of the eastern tropical Pacific (Roshan et al., 2017). This large difference in stoichiometry between the shallow and deep, or "kink" in the ratio, is observed across the global ocean. At the surface, preferential uptake of Cd relative to PO_4 can occur as a result of Fe and/or Zn seawater depletion (Cullen, 2006), with Fe-limited cells reducing surface Zn concentrations and continuing to take up Cd through biodilution (Sunda and Huntsman, 2000). Fe limitation additionally causes the up-regulation of nonspecific divalent metal transporters to which Cd competitively binds, further contributing to Cd drawdown from seawater (Cullen, 2006; Lane et al., 2008; Saito et al., 2010). Such distinct Cd : PO_4 stoichiometries can be transported into larger features, where exported high-latitude intermediate waters containing high Cd : PO_4 ratios mix with lower-latitude water masses containing low Cd : PO_4 (Baars et al., 2014; Frew and Hunter, 1995; Middag et al., 2018; Xie et al., 2015). In our data set, Antarctic-sourced seawater is evident by low excess Si, or Si* (Si – NO_3), which coincides with the change in slope, and displays a transitional Cd : PO_4 ratio (Fig. S4). Lateral differences in stoichiometry across the transect were furthermore demonstrated with a steeper Cd : PO_4 ratio of 597 pmol : µmol observed in deep water of the South Pacific (St. 9–13) compared to a slope of 472 pmol : µmol farther north (St. 1–8; Fig. 4c). We next contrast these trace metal distributions with hydrothermally influenced sites in the NE Lau Basin.

3.2 Hydrothermal activity in the southwest Pacific (St. 9–13)

Dissolved metal distributions in the lower transect are consistent with several local hydrothermal sources originating in the NE Lau Basin. δ^3He samples were not collected during the MetZyme expedition, and as a result, comparisons are made using prior δ^3He collected in the region. Most strikingly, a prominent dFe and dMn feature was observed at 15° S and 174.5° W (St. 13; Fig. 5a, b). Dissolved Fe and dMn steadily increased to 5.2 and 11.3 nM, respectively, by 1900 m, in contrast to typical bathypelagic concentrations of ∼ 0.5 nM dFe and ∼ 0.18 nM dMn at stations farther north. These maxima were located just 81 km east of a maximum δ^3He (43.4 %) centered at 1726 m, collected at 15° S and 173.1° W 2 decades prior (Lupton et al., 2004), and could be associated with a common hydrothermal source. Alternatively, an intense δ^3He signal of 58.7 % has been measured 168 km west of our site, at 15.64° S and 177.32° W, and centered at 1924 m and may also be associated with these metal anomalies, although seawater at this depth should advect to the northwest (Fig. S5) (Lupton et al., 2004; Reid, 1997; Speer and Thurnherr, 2012). Thus, that hydrothermal source is not expected to be responsible for the metal features to
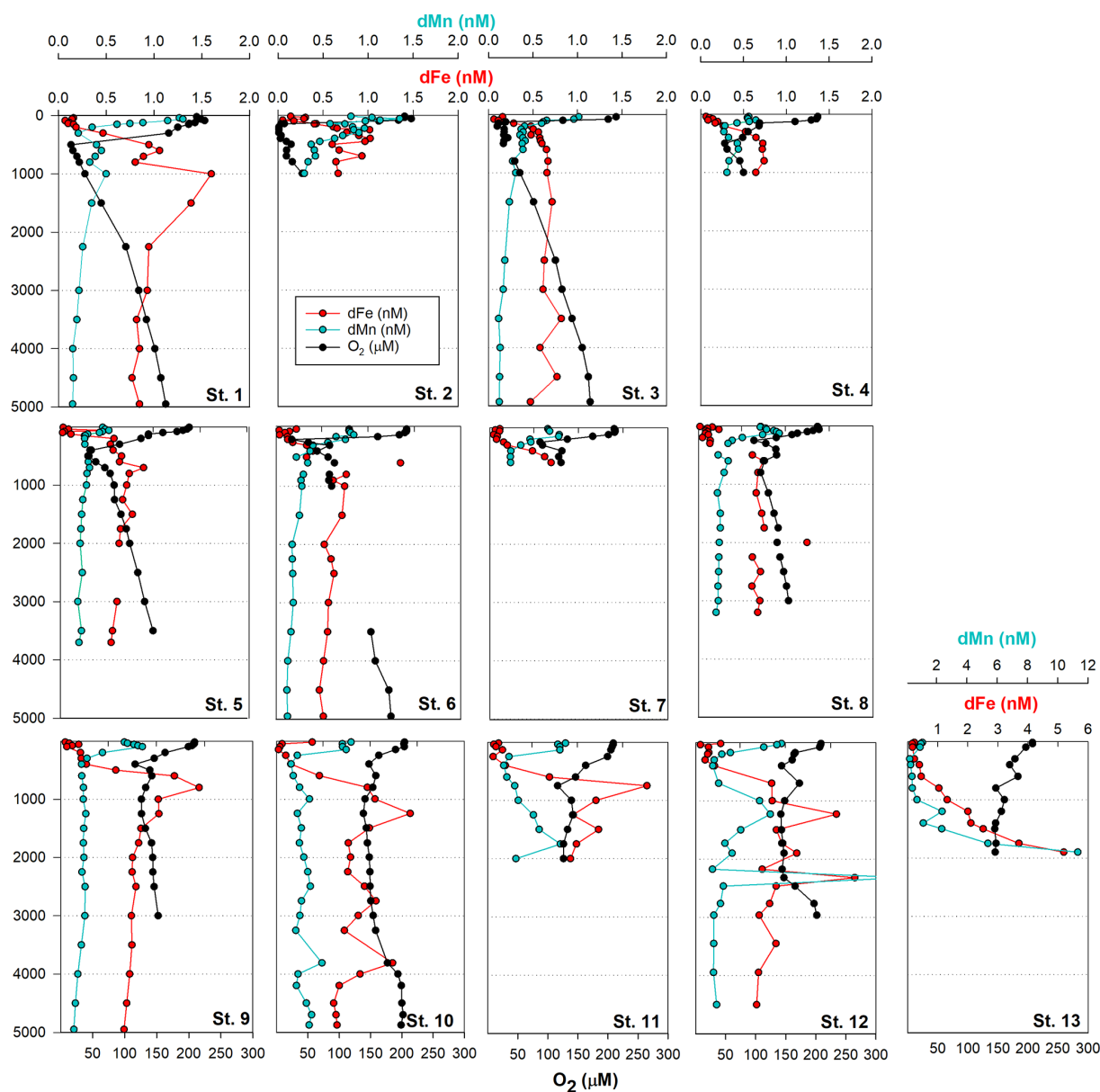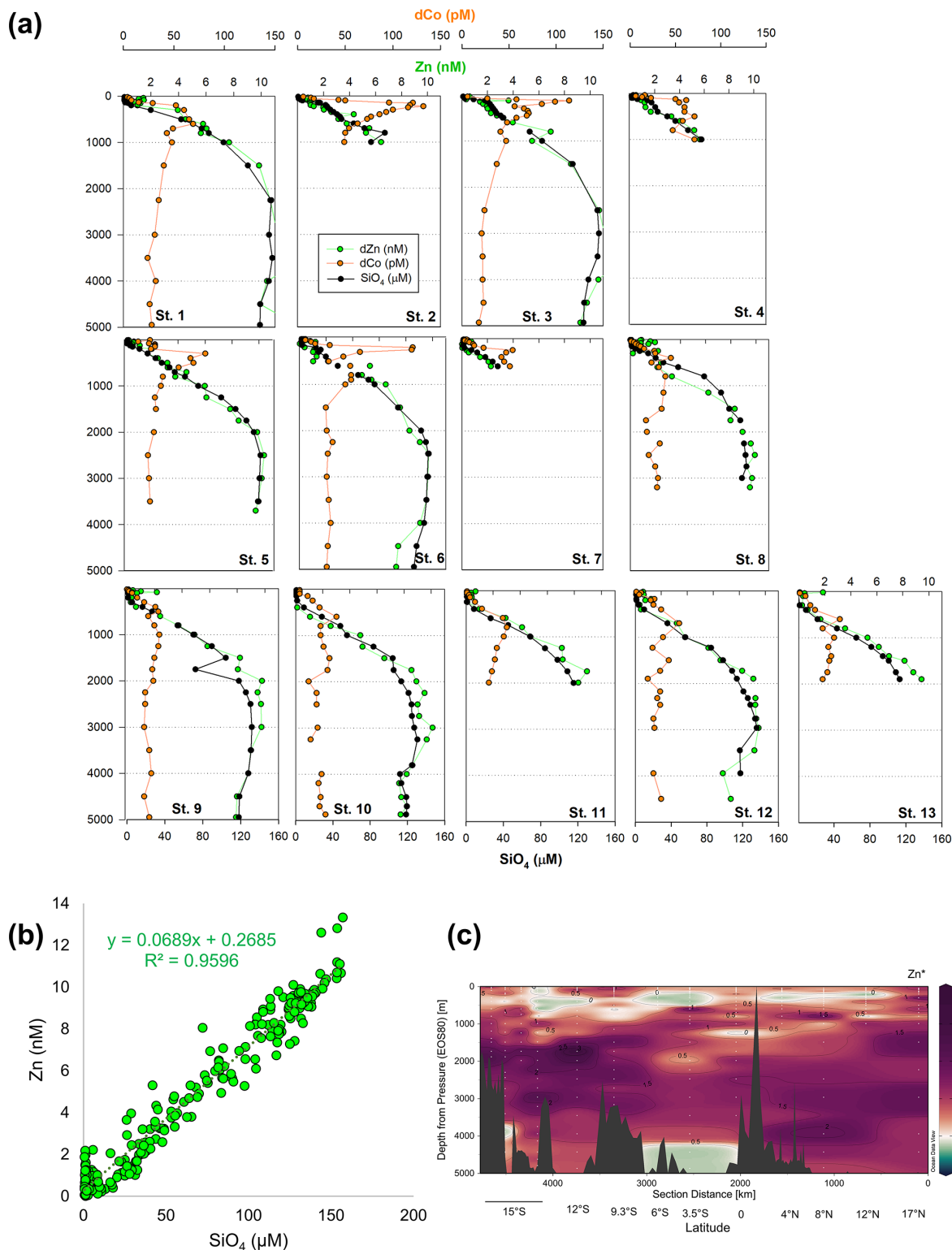
Figure 2. Full-depth metal profiles for dissolved Fe (red) and Mn (blue) and oxygen (black).

the east. No physiochemical signatures were detected using CTD sensors (temperature, salinity, turbidity), implying this was not a near-field hydrothermal-plume feature (Fig. S3).

The St. 13 dFe : dMn ratio of 0.43 at 1900 m is low compared to the distal plumes from the southern East Pacific Rise and Lo'ihi systems with ratios > 2 (Fitzsimmons et al., 2014; Jenkins et al., 2020), likely due to the distinct underlying geology in this back-arc setting. Hydrothermally derived Zn was evident with excess Zn (Zn*) in the vicinity, which demonstrated higher-than-expected Zn concentrations based on its relationship to Si (Zn − 0.053 × Si) and similar to observations made in the southern East Pacific Rise (Fig. 3c) (John et al., 2018; Roshan et al., 2016). Other trace metals

investigated (Cu, Ni, Co, Cd) did not show distributions consistent with a hydrothermal source (Fig. 1).

The NE Lau Basin is semi-enclosed, topographically restricted by the Tonga Ridge to the west and south, Lau Ridge to the west, and Zephyr Shoal below 2000 m to the north (Speer and Thurnherr, 2012). Distal plumes are therefore expected to vent to the northwest, consistent with circulation patterns measured from NE Lau Basin float trajectories (Speer and Thurnherr, 2012). Elevated dFe and dMn concentrations at St. 13 coincide with where the highest hydrothermal output is expected; north-bound hydrothermal outflow is steered along the east side of the Tonga Ridge before ultimately escaping into the northwest (Speer and Thurnherr,

Figure 3. (a) Full-depth metal profiles for dissolved Co (orange) and Zn (green) and silicate (black). **(b)** Dissolved Zn distributions are supported by a strong linear relationship with SiO_4 along the cruise transect, with a Zn : Si slope of 0.069 nmol : µmol and an R^2 of 0.96. **(c)** Zn* MetZyme section, or Zn − 0.053 × Si, displaying higher-than-expected Zn levels in the vicinity of the hydrothermal plume.
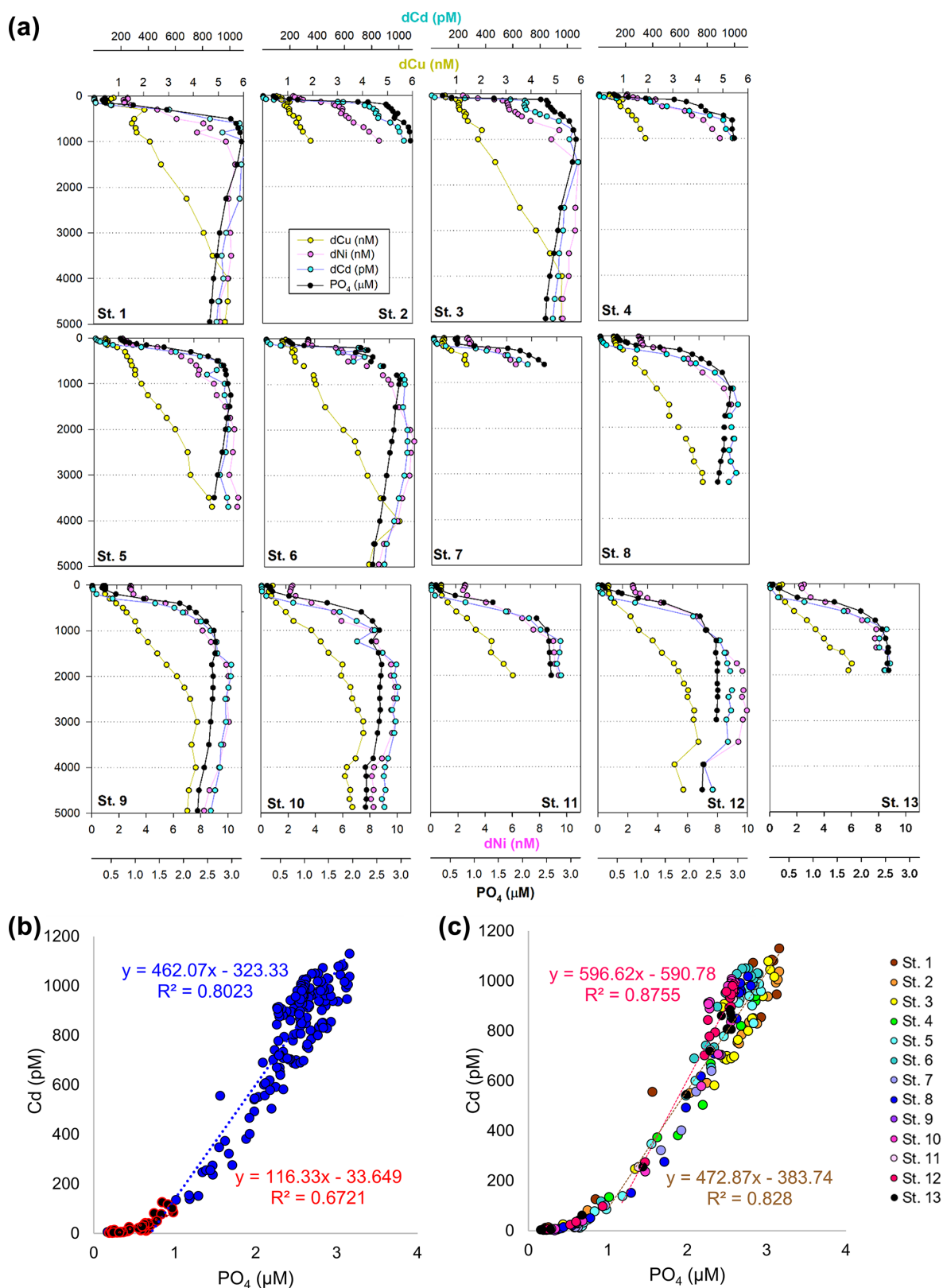
Figure 4. (a) Full-depth metal profiles for dissolved Cd (blue), Cu (yellow), Ni (pink), and phosphate (black). **(b)** Linear relationship between dissolved Cd and PO_4 across the transect, separated by shallow ($< 1\,\mu M$ PO_4; red) and deep ($> 1\,\mu M$; blue). **(c)** Cd and PO_4 relationship in the North Pacific compared to southwest Pacific. Cd : PO_4 relationship for St. 1–8 in deep water ($> 1\,\mu M$) is shown in brown; St. 9–13 ($> 1\,\mu M$) is shown in pink.
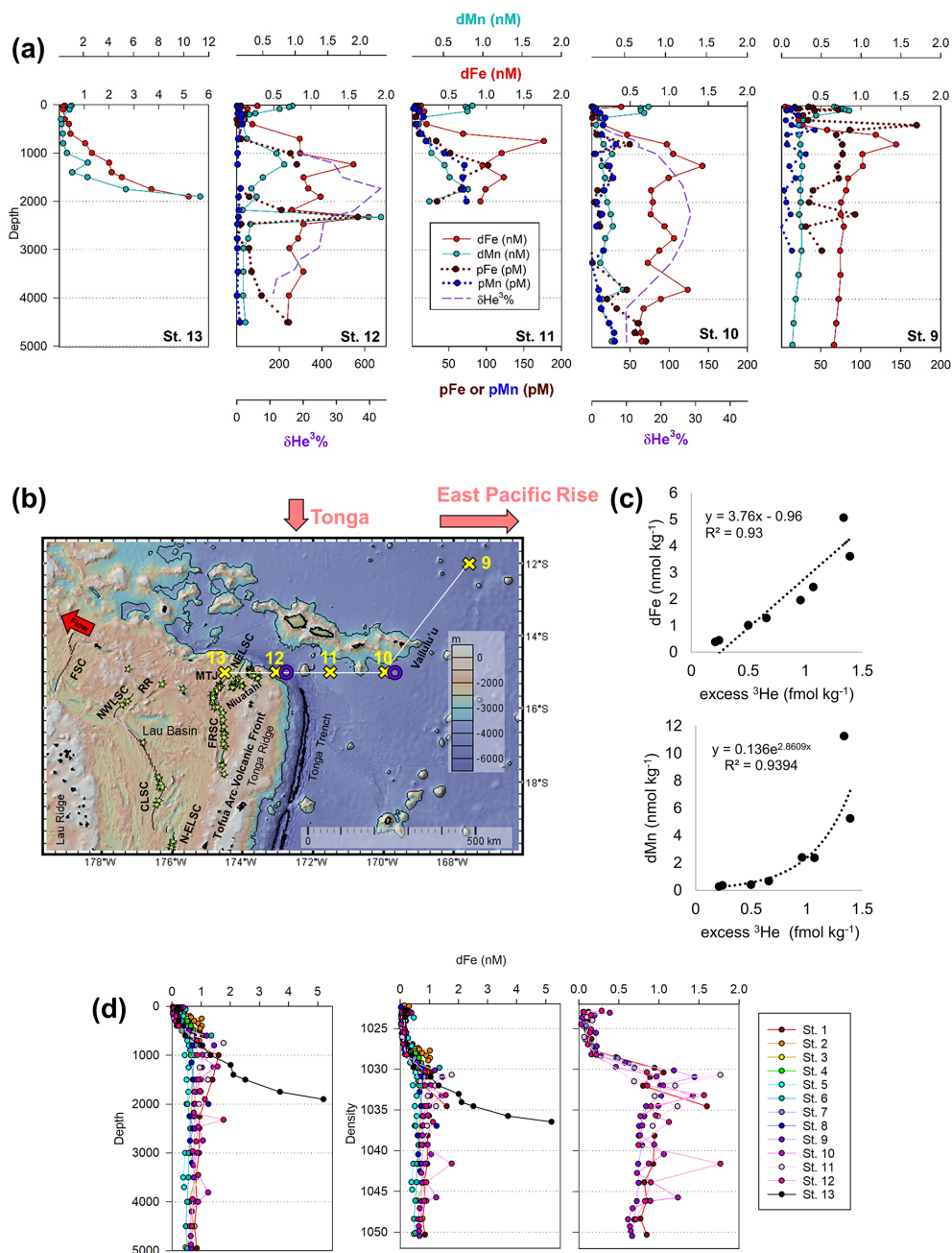
Figure 5. (a) Total dissolved Fe (red) and Mn (aqua) and particulate Fe (brown) and Mn (navy) alongside hydrothermal helium (purple) in the NE Lau Basin. Helium data were collected in 1987 and 1990 from identical locations as trace metals in 2011 (St. 10 and 12; Lupton et al., 2004). **(b)** The tropical southwest Pacific leg of the MetZyme transect (St. 9–13) in the northeastern Lau Basin, plotted using GeoMapApp. Nearby hydrothermal vent sites are indicated with green stars (Baker et al., 2019; Beaulieu et al., 2013), and spreading axes are labeled (Baker et al., 2019; Lupton et al., 2012; Martinez et al., 2006). The red arrow indicates direction of flow at 2000 m (Reid, 1997; Speer and Thurnherr, 2012). FSC: Futuna Spreading Center; NWLSC: Northwest Lau Spreading Center; RR: Rochambeau Rifts; CLSC: Central Lau Spreading Center; N-ELSC: northern Eastern Lau Spreading Center; FRSC: Fonualei Rift and Spreading Center; MTJ: Mangatolo Triple Junction; NELSC: Northeast Lau Spreading Center. **(c)** Estimated relationship between dissolved Fe or Mn and excess helium in the NE Lau Basin. Excess ^{3}He was calculated using δ^3He reported in Lupton et al. (2004) at the same coordinates as MetZyme St. 12 and metal concentrations from MetZyme St. 13. A Type II linear regression is shown for dFe (Glover et al., 2012); dMn showed a nonlinear relationship with excess ^{3}He better fit by an exponential trend line. Note that total He and Ne concentrations were not available and were estimated based on similar δ^3He and depth in the southwest Pacific using climatological data contained in the Global Oceanic Database of Tritium and Helium between 14–17° S and 160–180° W (Jenkins et al., 2019a). Upper-water-column excess ^{3}He concentrations were extrapolated using historical data from Lupton et al. (2004). **(d)** Dissolved iron profiles at each station plotted with depth (left) and density (right).

2012). This is similar to topographic steering of the Kairei plume along the Central Indian Ridge in the Indian Ocean (Rudnicki and German, 2002).

Farther east at St. 9–12, dFe and dMn profiles demonstrate additional hydrothermal sources showing lateral consistency ~ 300 km apart (Fig. 5a). As seawater at 2000 m advects in a northwestern direction (Lupton et al., 2004; Reid, 1997), it is unlikely that the sharp feature detected at St. 13 was contributing to elevated metal concentrations at these stations farther east (St. 9–12). They additionally reside in different density layers (Fig. 5d). Seawater samples collected during the MetZyme expedition from the identical location as the previously measured ^{3}He core (δ^3He $= 43.3$ %; Lupton et al., 2004) show two dFe and dMn peaks straddling the δ^3He maximum at 1726 m with a concave distribution (MetZyme St. 12). The shallower metal peaks occurred at 1230 m, with 1.6 nM dFe and 0.83 nM dMn, while the deeper peak consisted of 1.8 nM dFe and 2.3 nM dMn at 2320 m (Fig. 5b). These shallow and deep dFe and dMn signals are also present 333 km east of the Tonga Ridge at 15° S and 170° W (St. 10), where dFe and dMn were 1.4 and 0.22 nM, respectively, at 1243 m depth and 1.1 and 0.26 nM, respectively, at 2744 m (Fig. 5b). Although the St. 12 deep dFe signal is much sharper than the one at St. 10, the integrated areas of both peaks between 2000–3000 m are comparable (907 vs. 849 µmol m^{-2}, respectively), suggesting a similar iron supply, and they fall in the same density layer (Fig. 5d). Notably, particulate Fe (pFe) matches the dual dFe peaks and therefore supports two separate hydrothermal sources at St. 10 and St. 12 and demonstrates that particle formation and scavenging is not driving the concave dissolved Fe profile distributions. A third peak is present at St. 10 at 3803 m, where dFe reaches 1.24 nM and dMn 0.48 nM, and at St. 12 at 3450 m, where dFe reaches 0.9 nM, although the Lau Basin sea floor is not that deep, and neither signal could originate from there. A shallow dFe signal was furthermore captured at St. 11, where only a partial profile was obtained from the upper water column. Apart from multiple hydrothermal sources, sills may also explain the multi-featured metal profiles with seawater advecting away from the hydrothermal source(s) coming into contact with sill structures, disrupting flow and dispersing the plume in three dimensions (Fig. 1). Elevated subsurface dFe was evident as far north as St. 9 (12° S, 167.6° W), where dFe reached 1.4 nM at 800 m (Fig. 2).

As St. 9 is our northernmost station that captures hydrothermal influence in the dissolved metal fraction, we suspect that the plumes captured in this survey do not continue north and instead discharge laterally or to the northwest, where they escape to the tropical southwest Pacific. There was little evidence of the East Pacific Rise plume-derived dFe advecting west over ~ 6000 km in the St. 10 dFe profiles (Fig. 2a), despite the pronounced δ^3He of 30 % observed at 2500 m at this location (Lupton et al., 2004) and a dFe : ^{3}He signal evident just ~ 550 km south of this site (Fitzsimmons

et al., 2014). It is possible the St. 10 dFe peak at 2750 m is associated with the East Pacific Rise but likely that any East Pacific Rise-sourced Fe is overshadowed by the more intense local plumes at St. 12.

Our trace metal profiles are consistent with the presence of multiple, diverse sources of venting in this region of the NE Lau Basin (Baker et al., 2019) and exhibit changes in non-buoyant plume location, intensity, and/or depth in the water column compared to the ^{3}He anomalies that were more than 2 decades earlier, in 1987 (Lupton et al., 2004). The core of the ^{3}He plume identified by Lupton et al. (2004) was located at the same site as our St. 12, approximately 81 km east of where the strongest dFe and dMn signal was detected at our St. 13 (Fig. 5b). Furthermore in the original ^{3}He data set, there was no signal associated with shallow dFe and dMn enrichments at ~ 1200 m, where only the deeper δ^3He signature centered at 1726 m was apparent (Lupton et al., 2004). We hypothesize that these differences within the dynamic NE Lau Basin system may be due to changes in hydrography in the pathways and/or flux of the plume materials exiting the Lau Basin together with recognition that extensive new eruptions should be expected to have arisen along this fast-spreading back-arc system (up to 42 mm yr^{-1} full spreading rate; Baker et al., 2019) since the corresponding ^{3}He sampling was conducted in 1987. Multiple distinct hydrothermal vent sources appear responsible for the metal-rich plumes observed at different depths and density surfaces observed here, all of which should be expected to contribute to the larger excess ^{3}He pool (Fig. 5a) (German et al., 2006; Lupton et al., 2004).

The northeastern Lau Basin contains 135 active hydrothermal sites, with new sites continuing to be discovered (Fig. 5b; Baker et al., 2019; Beaulieu et al., 2013). The exact vent sources responsible for the dFe and dMn distributions observed here are unknown. The strongest metal plume signals in this study come from St. 13, which is < 50 km from the NE Lau Basin Spreading Center (NELSC) and the Mangatolo Triple Junction (MTJ), which have plume depths between 1300–2400 m (Fig. 5b) (Baker et al., 2019; Kim et al., 2009; Lupton et al., 2004). There is extensive arc volcanism to the east, which likely generates further complexity, with additional vents feeding multiple shallower plume depths (Baker et al., 2019; Staudigel et al., 2004, 2006). This is observed in dFe and dMn profiles from St. 12 eastward when compared to the broad coalesced plume that dominates ^{3}He distributions in the NE Lau Basin (Lupton et al., 2004). Although active hydrothermal venting has been measured east of the Tonga Arc at the Vailulu'u Seamount Samoan Island chain hotspot (Staudigel et al., 2004), this system is not likely responsible for the intense ^{3}He plume given that the maximum ^{3}He signal is located within the W–E lateral bounds of the Lau Basin (Lupton et al., 2004) and that the St. 13 metal plume falls along the ridge axis (Fig. 5b). The Vailulu'u Seamount additionally has a crater depth of just

750 m (Staudigel et al., 2004), which is too shallow to explain the strong metal-enriched feature we report here at 1900 m.

Using metal concentrations from St. 13 and δ^3He quantified by Lupton et al. (2004) from our St. 12, we estimate the maximum amount of dFe relative to excess ^{3}He released from this back-arc setting (Fig. 5c, Table 3; for comparison, the relationship between St. 12 dFe and ^{3}He is shown in Fig. S6). St. 13 dFe showed a linear relationship with ^{3}He with a slope of 3.8×10^6, while dMn, in contrast, behaved non-conservatively. Geostrophic flow supports northwest circulation at this depth (Lupton et al., 2004; Reid, 1997; Speer and Thurnherr, 2012), and dFe : ^{3}He ratios of 3.8×10^6 represent a significant source of Fe being introduced to microbial communities at bathypelagic depths in this direction. The dFe : ^{3}He estimates for this back-arc area (Table 3) are distinct from but comparable to what has previously been reported for other major plumes at a mid-ocean ridge (southern East Pacific Rise, EPR) and an intra-plate hotspot (Lo'ihi Seamount) (Fitzsimmons et al., 2017; Jenkins et al., 2020). Our metal data demonstrate that the hydrothermal plume observed by Lupton et al. (2004) has the capacity to export large amounts of Fe and Mn to the ocean interior, similar to the southern EPR and Lo'ihi systems (Jenkins et al., 2020; Resing et al., 2015). We next discuss how microbial physiology may have been impacted by this distal plume.

3.3 Microbial community composition in background and hydrothermally influenced seawater

The influence of distal hydrothermal-plume geochemistry on surrounding microbial physiology and ecology was assessed using comparative metaproteomics with the 3–51 μm fraction of the MetZyme meta-omic data set (Cohen et al., 2021a). Since hydrothermal vents were not the focus of this expedition, real-time instrumentation for tracking hydrothermal signatures was not on board the ship. Instead, seawater samples and biomass were collected at the same location where hydrothermal activity had been observed previously, at St. 12 (Lupton et al., 2004), and analyzed back in the laboratory. We therefore were unaware that the largest metal signatures were at St. 13 or that present-day plume maxima at St. 12 were at 1200 and 2200 m, and so biomass was not collected at these depths. However, biomass *was* obtained in the vicinity of hydrothermal influence, at St. 12 (15° S, 173.1° W) at 1900 m, where dissolved and particulate metals were higher than background concentrations. Other deep (≥ 200 m) samples collected across the transect served as background, non-hydrothermally influenced vent sites ($n = 20$). MetZyme metaproteomes from the upper water column are used comparatively to the deep ocean but are not the focus of this analysis.

Microbial communities collected on the 3–51 μm filters were composed of archaea, heterotrophic bacteria, viruses, cyanobacteria, protists, and metazoans (Fig. 6). In particular, dinoflagellates, Alphaproteobacteria, and *Prochlorococ-*

cus accounted for an average of 50 ± 9 % (± 1 standard deviation) across all of the sample communities based on NSAF-normalized proteins (Fig. 6). The presence of prokaryotic organisms smaller than 3 μm represents particle-associated assemblages, filamentous chains, host-symbiont relationships, or cells aggregated or adsorbed onto biomass-dense filters. Samples collected from the upper water column (< 200 m) showed higher proportions of cyanobacteria, while relative distributions of the other abundant groups, including Gammaproteobacteria and Alphaproteobacteria, were more abundant with depth (Cohen et al., 2021a). Although the 0.2–3 μm fraction would certainly contain pelagic bacteria and archaea sensitive to hydrothermally derived chemical species, we were not able to extract enough biomass from this filter fraction for the metaproteomic analysis.

Amplicon sequencing of ribosomal RNA was used to determine community composition along the MetZyme transect (Cohen et al., 2021a). A PCoA analysis constructed with 18S and 16S rRNA operational taxonomic units (OTUs) demonstrated that the eukaryotic and prokaryotic communities at the hydrothermal site largely resembled that of background locations (Fig. S7). These similarities between the distal-plume-influenced and background prokaryotic communities agree with findings from buoyant hydrothermal plumes at vent-sites along the Eastern Lau Spreading Center (ELSC), where it has been argued that microbes sourced from background seawater are entrained into and displace seafloor organisms (Sheik et al., 2015). Deep-sea communities therefore may be relying on metabolic plasticity to exploit a variety of environmental conditions, enabling the occupation of both hydrothermal and non-hydrothermal influenced seawater systems. Protistan groups such as ciliates, stramenopiles, dinoflagellates, and radiolarians are also ubiquitous in the deep ocean and may serve as important vectors for transferring carbon obtained from vent sites to the broader bathypelagic ocean (Mars Brisbin et al., 2020; Murdock and Juniper, 2019; Olsen et al., 2015). However, hydrothermal populations can be genomically distinct from background communities at a fine taxonomic level, which has been observed in vent-influenced protistan communities using amplicon sequence variants (ASVs) (Hu et al., 2021; Mars Brisbin et al., 2020) and bacterial functional genes (Mino et al., 2013, 2017), although this was not observed here using an OTU approach. Interestingly, disconnects between the amplicon and proteomic data sets were apparent, with the 16S rRNA analysis indicating that cyanobacteria were one of the most relatively abundant taxa identified even in deep waters (≥ 200 m; Fig. S8), while < 25 % of deep prokaryotic proteins belonged to cyanobacteria (Fig. 6). Such differences could be due to extraction, primer, and/or sequencing bias (Brooks et al., 2015; VerBerkmoes et al., 2009); limited references in taxonomic databases (Orellana et al., 2019); or biological differences in cellular pools of RNA and proteins. Regardless, both analyses indicate that at a coarse taxonomic level, particle-associated prokaryotic

Table 3. Dissolved-metal-to-excess-^{3}He ratios among the NE Lau Basin, Lo'ihi Seamount, and southern East Pacific Rise distal plumes. The NE Lau Basin ratio was calculated here using δ^3He reported by Lupton et al. (2004) from the same location as MetZyme St. 12 and using MetZyme St. 13 dissolved metal concentrations. No upper-water-column ^{3}He values were available for 400–800 m, and they were therefore linearly extrapolated. Excess ^{3}He was determined following the equation in Jenkins et al. (2020). The Type II linear regression slope is shown for dFe. St. 13 dMn showed a nonlinear relationship with excess ^{3}He better fit by an exponential trend line. Note that He and Ne concentrations were not available from Lupton et al. (2004) and were instead estimated based on similar δ^3He values and depths in the Global Oceanic Database of Tritium and Helium (Jenkins et al., 2019a) between 14–17° S and 160–180° W. Helium isotope solubility fractionation factors, He and Ne solubilities, and Type II regressions were calculated using *healph*, *LJSolMol*, and *lsqfitma* MATLAB functions (Jenkins et al., 2019a, b, 2020). The dFe : ^{3}He ratios were obtained from the regression of individual samples at one site.

	NE Lau Basin (this study)	Lo'ihi Seamount (Jenkins et al., 2020)	East Pacific Rise (Fitzsimmons et al., 2017)
dFe : ^{3}He	3.8×10^6	4.4×10^6	4.3×10^6
dMn : ^{3}He	$0.14e^{(2.86x)}$	1.0×10^6	2.3×10^6

and microeukaryotic communities in this size fraction at the hydrothermal site were similar to those of background seawater.

3.4 Metaproteomics of particle-associated microbial communities in hydrothermally influenced seawater

Metaproteomics was performed by injecting purified peptides from each station and depth onto a liquid chromatography system in two-dimension active modulation mode coupled to an Orbitrap mass spectrometer running in data-dependent acquisition (DDA) mode (see "Methods") (McIlvin and Saito, 2021). The full data set contains 9796 proteins, 99 143 peptides, and 366 025 total spectral counts, of which 80 % of the proteins have a taxonomic and/or functional annotation (Cohen et al., 2021a). To investigate metabolically active proteins influenced by hydrothermal metal release, a permutation test was performed with only deep samples (≥ 200 m, $n = 21$), comparing background non-hydrothermally influenced vent sites ($n = 20$) to a single site within the vicinity of a hydrothermal plume (St. 12, 1900 m). A two-tailed asymptotic general independence test was used followed by Benjamini–Hochberg p value correction (FDR < 0.1). Of the 3492 deep (≥ 200 m) proteins, 201 were either more abundant at the hydrothermal site compared to background sites or solely identified at the hydrothermally influenced site (FDR < 0.1; Table S2). Consistent with the amplicon sequencing analysis, the taxonomic identity of hydrothermal-plume-associated proteins largely resembled that of background sites; 84 % of these hydrothermally influenced proteins belonged to the particle-associated prokaryotes. Of the 201 proteins enriched at the hydrothermal vent site, 169 were prokaryotic, 28 eukaryotic, and 4 viral (*Prochlorococcus* phage P-SSM2 and P-SSP7; *Synechococcus* phage S-RSM4; Fig. 6). The implications of hydrothermal activity on microbial metabolism were next explored by examining differentially abundant proteins involved in metal transport, amino acid metabolism, and chemoautotrophy.

3.5 Microbial trace metal and organic transporters, structural proteins, and proteases potentially utilized in the dispersing plume

A number of transporters identified may aid in uptake and efflux of metals and organics originating from the hydrothermal plume. These include a heavy metal transporter protein belonging to the Betaproteobacteria Burkholderiales family which was not detected outside plume-influenced seawater (FDR = 3×10^{-4}; Fig. 6). Although trace metals are micronutrients required by cells to carry out essential biochemical reactions, high concentrations lead to oxidative stress and cell damage. Therefore, this protein may be useful for either uptake or efflux out of the cell. Bacterial TonB outer membrane receptor proteins were investigated as they are involved in transport of siderophores, inorganic metals, vitamin B_{12}, and carbohydrates (Noinaj et al., 2010). The majority of TonB proteins identified were not differentially abundant ($n = 83$, Fig. 7), although three in particular were enriched in the vicinity of the plume. Two of these TonB proteins were fourfold (FDR = 3×10^{-4}) and sixfold (FDR = 0.006) more abundant in the plume and belonged to the Flavobacteriales family within Bacteroidetes. One contained the SusC and CirA domains characteristic of carbohydrate and inorganic Fe uptake, respectively, and the other contained the SusC, B_{12} (BtuB), and FepA siderophore domains. An additional TonB protein was ninefold more abundant in the hydrothermal plume (FDR = 0.006), belonging to the Alteromonadales family within Gammaproteobacteria and containing the BtuB domain. Although TonB genes are highly expressed in Gammaproteobacteria from the Guaymas Basin hydrothermal plume (Li et al., 2014), we did not find evidence for overall enrichment, with only these 3 out of 83 TonB transporter proteins identified as differentially abundant in the plume, suggesting that these transporters are broadly utilized by deep-sea bacterial communities. The
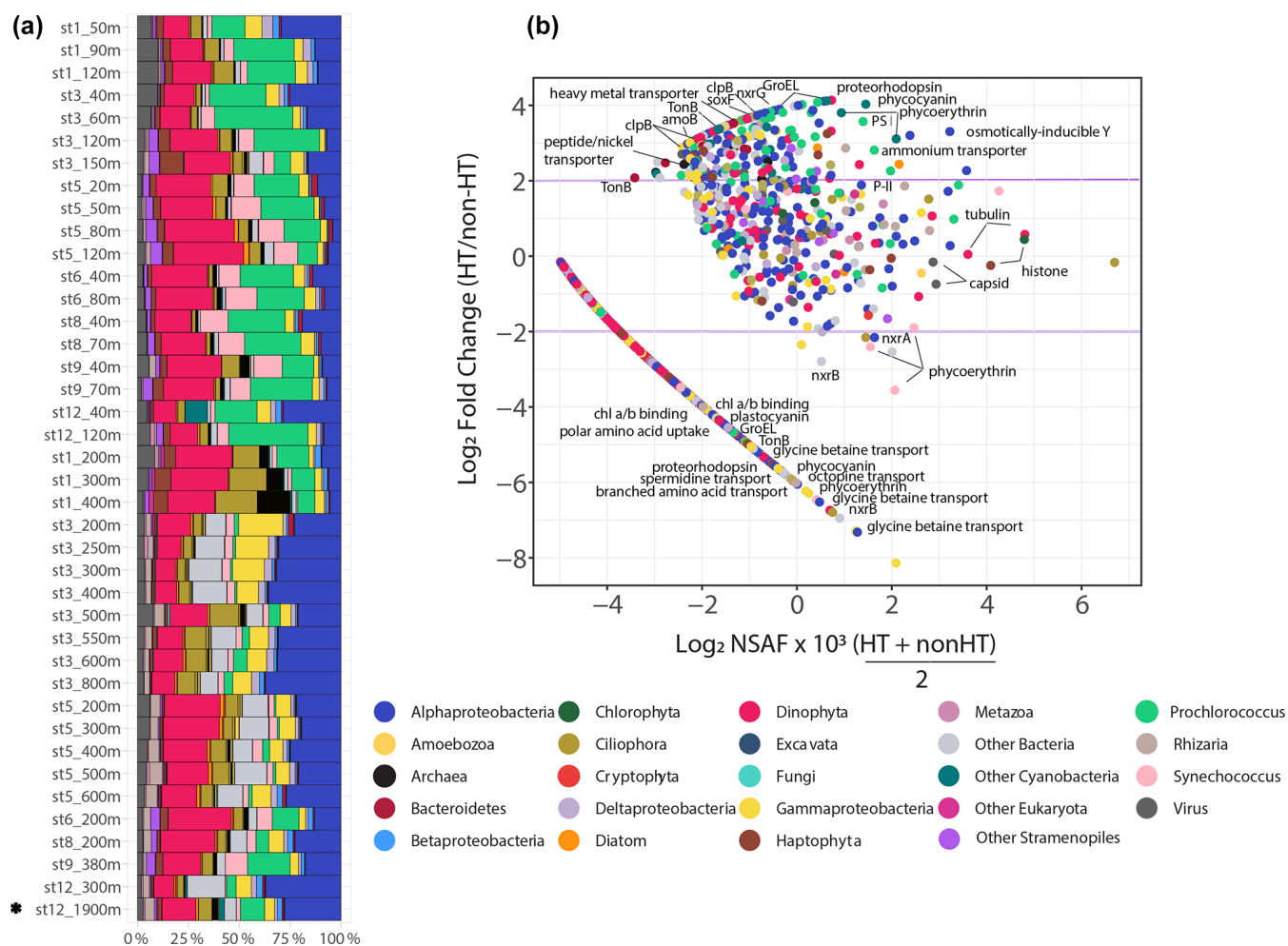
Figure 6. Whole-community phyla and supergroup-level relative community abundance determined through metaproteomics on the 3–51 µm size fraction, modified from Cohen et al. (2021a) **(a)**. Only peptide spectral counts matching open reading frames (ORFs) with a classified taxonomic annotation and lineage probability index greater than 0.7 are shown. Exclusive spectral counts were normalized following the NSAF (normalized spectral abundance factor) approach. Differential abundance of proteins in the hydrothermal plume (St. 12, 1900 m) compared to non-hydrothermal background deep sites ($n = 20$) **(b)**. The x axis represents relative protein abundance (NSAF-normalized spectral counts), and the y axis is the $\log_2$ fold change in protein abundance between the hydrothermally influenced site (St. 12, 1900 m) and the average of deep (≥ 200 m) background sites ($n = 20$). The horizontal purple lines mark a $\log_2$ fold change of 2 or -2 for a fourfold increase or decrease in protein abundance, respectively. A small value of 0.03 was added to normalized spectral counts to allow for log transformation. Linear arm contains proteins not identified in the hydrothermal plume. Note that not all protein groups of interest are annotated; for a complete list of key proteins identified see Fig. 4 and Table S2. (Nxr: nitrate oxidoreductase; SoxF: sulfur oxidation protein; Amo: ammonia monooxygenase; PS I: photosystem I reaction center protein).

three that are specific to the hydrothermal plume may belong to bacterial strains that were relatively more abundant in the plume environment or that contain protein isoforms with distinct functional roles. Two of nine putative ABC transport system siderophore transporters belonging to Rhizobiales Alphaproteobacteria and Vibrionales Gammaproteobacteria were additionally enriched in the plume-influenced seawater (FDR $= 3 \times 10^{-4}$ and 9.7×10^{-4}, respectively). These elevated siderophore transporters may be consistent with increased ligand production in plumes, as has been invoked

in stabilizing hydrothermal Fe through organic complexation (Bennett et al., 2008).

Similar to the TonB transporters, NikA nickel and/or metallophore ABC transporters, used for the uptake of metals or oligopeptides, are ubiquitous in the deep ocean (Fig. 7). Three NikA subunit proteins however were differentially abundant in the plume; two belonged to Rhizobiales Alphaproteobacteria and one to Thermoplasmatales archaea and were 10-fold (FDR $= 3 \times 10^{-4}$), 9-fold (FDR $= 0.01$), and 5-fold (FDR $= 0.01$) more abundant in the plume, respectively. The Nik ABC transport system may import Co

as well as Ni (Rodionov et al., 2006), and it is unknown whether Mn may also be imported through this uptake system or whether high concentrations of hydrothermal Mn could competitively inhibit Ni and/or Co uptake. Finally, a sodium/solute family symporter specific to acetate and belonging to SAR 11 Alphaproteobacteria was eightfold more abundant at the hydrothermal site (FDR = 3×10^{-4}), with this family of transporters also enriched in transcripts at Guaymas Basin (Dick et al., 2013). This collection of transport proteins reflects potential mechanisms for importing or exporting metals and organic resources sourced from the NE Lau Basin distal hydrothermal plume.

Protein-folding components and proteases were elevated in the plume and suggest a concerted effort to maintain cellular structure and utilize organic nitrogen. A total of 21 of 115 globally detected GroEL chaperone proteins involved in protein folding were relatively abundant at 1900 m (FDR < 0.1), belonging to Rhodobacterales, Rhizobiales, and PS1 clade members of the Alphaproteobacteria, Legionellales Gammaproteobacteria, Poribacteria, Planctomycetes, Chloroflexi, and cyanobacteria (Fig. 7). Microbes residing in hydrothermal systems are acclimated to extreme temperature and pressure (Merino et al., 2019), and chaperone GroEL proteins are hypothesized to be advantageous to thermophilic hydrothermal vent bacteria requiring a structural defense against the high-temperature environment, which can lead to protein misfolding (Chen et al., 2013; Wei and Zhang, 2010). As this was a distal hydrothermal plume at ambient temperature, the identification of these proteins may represent residual proteins from microbial communities that were transported from near-field vent sites during plume mixing and seawater entrainment. In addition, four of eight Clp proteases were solely detected in plume-influenced seawater, belonging to Alteromonadales and Vibrionales Gammaproteobacteria and Chloroflexi (FDR = 3×10^{-4}). Clp proteases are multi-subunit adenosine triphosphate (ATP)-dependent proteins that are found in diverse microorganisms including hyperthermophilic bacteria (Ward et al., 2002). Hydrothermal vents support dense chemosynthetic populations producing organics that may be accessed by heterotrophs using such proteases (Bennett et al., 2013; Dick, 2019). These proteases were not present at surveyed OMZs across the transect, and Clp protease gene expression was similarly uniquely elevated at the Guaymas Basin hydrothermal vent and not in the Eastern Tropical South Pacific (ETSP) OMZ (Dick et al., 2013). This protease therefore may be specific to hydrothermal-plume-associated heterotrophs.

Amino acids in particular can be stabilized in reducing, metal-rich, and acidic vent environments (Fuchida et al., 2014), and hence they may also be entrained into dispersing hydrothermal plumes. Certain amino acid transporters were relatively abundant in the plume-influenced seawater and may play a role in directly importing labile amino acids from the plume, including four branched and one L-amino acid transporters belonging to members of Alphaproteobac-

teria and Gammaproteobacteria (FDR ≤ 0.03). Heterotrophic plume microbes therefore appear to reinforce cellular structure using chaperone proteins, import amino acids, and express peptidases to potentially take advantage of available organic material.

3.6 Chemoautotrophy

Chemoautotrophic metabolism was detected in the plume with ammonium, nitrite, and sulfur oxidation proteins present. Many of these proteins were also present at OMZ sites and elsewhere along the transect, supporting widespread chemoautotrophy in the deep ocean (Fig. 7). One of three ammonia monooxygenase proteins (AmoB) belonging to Thaumarchaeota was sixfold more abundant in the plume (FDR = 0.07; Fig. 6). These transcripts are similarly elevated in hydrothermal systems (Baker et al., 2012), and genes are present in metagenome-assembled genomes of the eastern Lau Basin (Anantharaman et al., 2016). Thaumarchaeota is known to carry out ammonia oxidation in this region of the central Pacific (Santoro et al., 2017), and this process is not unique to hydrothermal plumes. One of 31 detected nitrite oxidoreductases, predicted to bind molybdenum and responsible for the conversion of NO_2 to NO_3 (NxrG), was attributed to the Brocadiales family within Planctomycetes and was relatively abundant in the plume and detected only at this location (FDR = 3×10^{-4}). These distributions support nitrification as a ubiquitous chemoautotrophic strategy (Pachiadaki et al., 2017; Saito et al., 2020), although chemoautotrophs likely have a competitive advantage over heterotrophs in low-organic, reducing environments with elevated ammonium and nitrite that can be oxidized as energy sources (Dick et al., 2013). Sulfur oxidation was potentially occurring, with SoxF belonging to Rhodobacterales Alphaproteobacteria only detected in the plume-influenced seawater (FDR = 3×10^{-4}). However, this SoxF protein was also present in surface waters (< 200 m) throughout the central Pacific transect and may also be utilized by heterotrophic bacteria residing in oxygenated waters performing anaplerotic inorganic carbon fixation via sulfur oxidation (Muthusamy et al., 2014). Other sulfur oxidation proteins known to be relatively abundant in the hydrothermal plume metatranscriptome were not detected (SoxA, DsrA) (Anantharaman et al., 2016; Dick et al., 2013). Metals and sulfide derived from vent fluid likely formed inorganic metal-sulfide clusters, reducing metal toxicity in the microbial community (Edgcomb et al., 2004) and limiting the bioavailability of sulfide to sulfide-oxidizing organisms, as observed in the Eastern Lau Spreading Center (Hsu-Kim et al., 2008; Sheik et al., 2015). Supporting this possibility, polymetallic massive sulfides have been observed in the NE Lau Basin (Beaulieu et al., 2013; Hawkins, 1986). Lastly, heterotrophic Mn-oxidizing bacteria are a major conduit for Mn oxide precipitation in non-buoyant plumes (Cowen et al., 1990). Multicopper oxidase enzymes responsible for heterotrophic
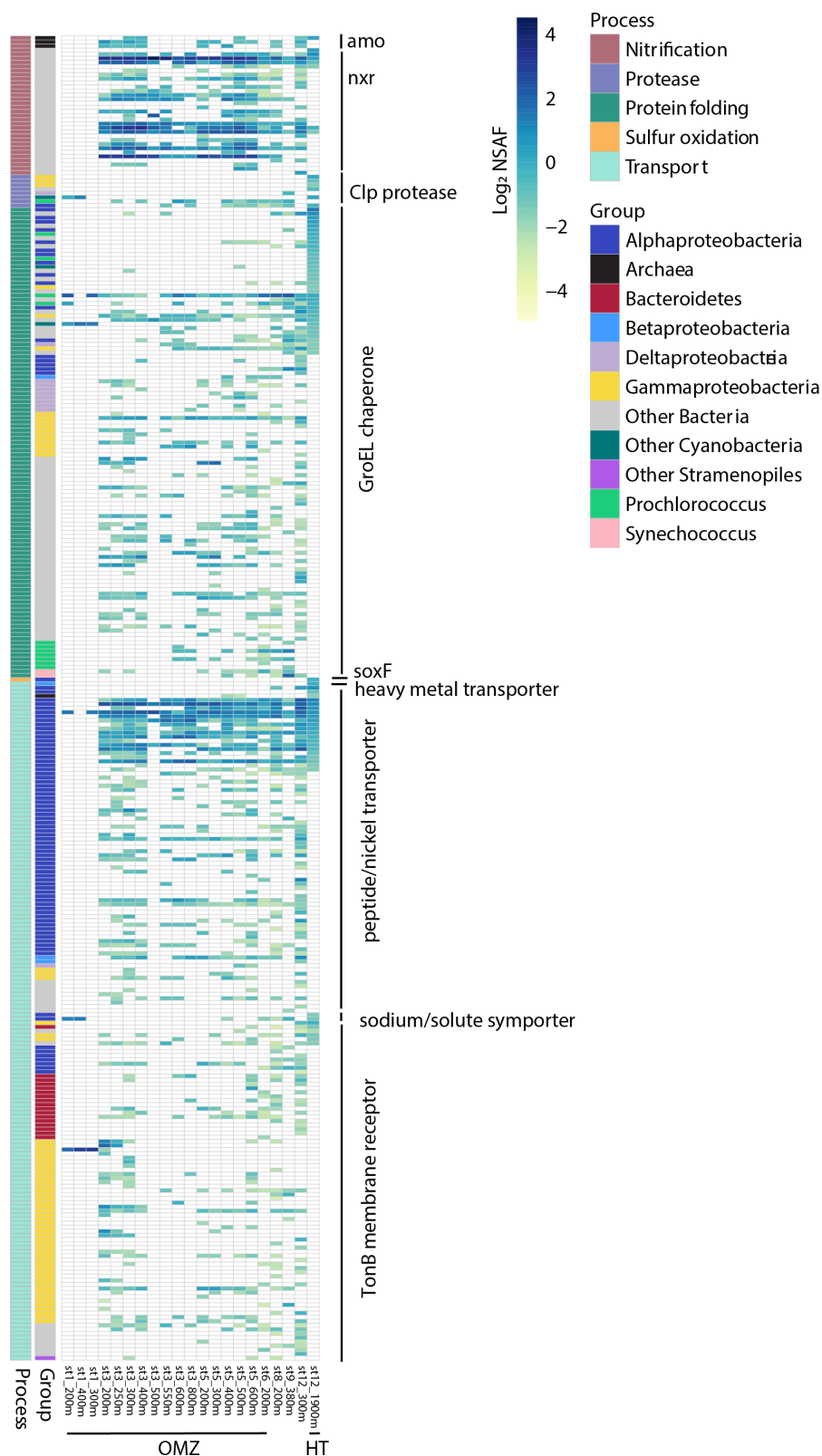
Figure 7. Heatmap displaying relative protein abundance for all proteins detected involved in chemoautotrophy, protein degradation, protein folding, and resource transport. Each row represents a unique protein with associated normalized spectral counts. White represents no protein detection. The sample collected from the hydrothermal plume (HT; St. 12, 1900 m) is shown alongside other deep samples ($\geq$ 200 m) collected along the MetZyme transect, including those within the OMZ region (St. 1–6, $\sim$ 150–1000 m). See Table S2 for the full list of proteins and annotations.

Mn oxidation in cultured hydrothermal bacteria (Dick et al., 2006), however, were not detected in the plume-influenced sample. Lithotrophic Mn oxidation is also theorized to occur in Mn(II)-rich vent fluids (Templeton et al., 2005) and has recently been described for the first time in Nitrospirae bacteria of tap water, which show high 16S rRNA sequence similarity to Nitrospirae from Lo'ihi Seamount seafloor lava (Yu and Leadbetter, 2020). In this analysis, Nitrospirae proteins were not enriched in distal-plume-influenced seawater ($> 3\,\mu$m fraction), though proteins of this phylum were detected elsewhere in the transect. Genes expressed in Nitrospirae and hypothesized to play a role in lithotrophic Mn(II) oxidation, including outer membrane c-type cytochromes and porin-cytochrome c complexes (Yu and Leadbetter, 2020), were similarly not enriched. It is possible that deep-sea Mn oxidation proteins differ from those characterized in our reference databases and are therefore missed during bioinformatic annotations.

3.7 Potential vertical transport of surface phytoplankton

The majority of photosynthetic proteins detected were highly represented in surface waters and included the pigments phycoerythrin, phycocyanin, and chlorophyll a-binding proteins as well as photosynthetic carbon fixation components flavodoxin and carbon concentrating proteins. Unexpectedly, a portion of differentially abundant proteins in the hydrothermally influenced seawater (at 1900 m) compared to background deep sites belonged to *Prochlorococcus* (20 %), and several light-associated proteins were differentially abundant, including phycoerythrin, phycocyanin, photosystem I subunit XI, chlorophyll a/b-binding proteins, proteorhodopsin, and RuBisCO (Fig. 6). The abundance of these proteins may represent metabolically active phototrophic cells maintaining core metabolism while rapidly sinking to the deep ocean, attached to larger particles in the 3–$51\,\mu$m size range, similar to fast-sinking, healthy diatom cells being detected at 4000 m in the Indian, Atlantic, and Pacific oceans (Agusti et al., 2015). There is furthermore growing support for fresh dissolved organic material (DOM) being exported to the deep ocean (Bergauer et al., 2018; Kirchman, 2018). It is unclear if these phytoplankton cells in deep waters are photosynthetically viable or partially degraded. Photosynthetic green sulfur bacteria have been isolated from a deep-sea hydrothermal vent in the East Pacific Rise, and it has been argued that these organisms use geothermal radiation as a light source (Beatty et al., 2005; White et al., 2002). The possibility of geothermal light biochemically stimulating photosynthetic proteins from sinking cyanobacterial cells warrants further exploration. Contamination cannot be completely ruled out but is unlikely to be solely responsible for the 1900 m protein biomass signal as approximately 23 L of surface seawater would be required to passively move through the 1900 m filter during vertical transport to pro-

duce the protein levels collected (Table S1). Future experiments will benefit from replicated biomass collection with large volumes filtered and examinations into the degradation state of proteins at depth.

4 Conclusion and outlook

This study represents the first metaproteomic assessment of deep-sea microbial communities in a dispersing hydrothermal plume and will be valuable in generating hypotheses regarding hydrothermal-plume carbon cycling, food web structure, and metabolic plasticity of deep-sea microbial communities. There are several recommendations that can be made for future studies evaluating microbial metabolism in distal-plume environments. (1) Performing meta-omics on distal plumes is challenging, and real-time tracking of hydrothermal features on board the research vessel is recommended to ensure optimal locations and depths are sampled. Meta-omic analyses in future studies will benefit from sample collection guided by in situ optical and redox sensors to maximize the biological signal that might be expected from samples taken toward the plume core. For example, investigations into metaproteomes of microbes residing in a metal-rich plume's center may reveal additional metal uptake, oxidation, or efflux proteins and processes not identified here. (2) In this study, we focused on particle-associated bacteria and protists collected onto 3–$51\,\mu$m filters. These findings may differ from the functionality of pelagic bacteria ($< 3\,\mu$m) inhabiting hydrothermal-plume environments. It is therefore recommended to survey both communities in future studies to ensure a comprehensive assessment of plume dynamics. (3) Finally, differences in taxonomic composition of microbial communities between hydrothermally influenced sites and background seawater were not observed using the 16S and 18S rRNA amplicon sequencing and metaproteomic approaches described here, although communities may be taxonomically distinct at a lower classification level. In particular, longer target regions and greater sequencing depth could provide enhanced resolution revealing differences in genera, species, or strains.

In summary, trace metal distributions along the central Pacific Ocean reflect a combination of biogeochemical influences, including biological uptake in surface waters, dissolution and decreased metal oxide production in OMZs, heterotrophic remineralization, scavenging at depth, and hydrothermal inputs. In the NE Lau Basin, several distinct hydrothermal plumes sourced from local spreading centers or volcanoes were observed. Hydrothermal dFe and dMn escapes into the tropical southwest Pacific in distal plumes, transporting metals to the surrounding bathypelagic ecosystem with a dFe : ^{3}He ratio that approaches that of the Lo'ihi and southern East Pacific Rise distal plumes. The communities within the plume taxonomically resembled those of non-hydrothermal sites, perhaps indicative of background seawa-

ter that is entrained into deep-sea hydrothermal plumes. Although protein signatures were largely similar between the hydrothermal plume and background locations, there were indications of altered microbial physiology with the differential abundance of proteins involved in metal transport, protein folding, and peptide degradation. The collection of proteins identified here offers a glimpse into hydrothermal vent metabolisms and expands our understanding of biogeochemical processes within basin-scale dispersing hydrothermal plumes and their influences on microbial physiology.

References

Agusti, S., Gonzalez-Gordillo, J., Vaque, D., Estrada, M., Cerezo, M. I., Salazar, G., Gasol, J. M., and Duarte, C. M.: Ubiquitous healthy diatoms in the deep sea confirm deep carbon injection by the biological pump, Nat. Commun., 6, 1–8, https://doi.org/10.1038/ncomms8608, 2015.

Anantharaman, K., Breier, J. A., and Dick, G. J.: Metagenomic resolution of microbial functions in deep-sea hydrothermal plumes across the Eastern Lau Spreading Center, ISME J., 10, 225–239, https://doi.org/10.1038/ismej.2015.81, 2016.

Baars, O., Abouchami, W., Galer, S. J. G., Boye, M., and Croot, P. L.: Dissolved cadmium in the Southern Ocean: Distribution, speciation, and relation to phosphate, Limnol. Oceanogr., 59, 385–399, https://doi.org/10.4319/lo.2014.59.2.0385, 2014.

Baker, B. J., Lesniewski, R. A., and Dick, G. J.: Genome-enabled transcriptomics reveals archaeal populations that drive nitrification in a deep-sea hydrothermal plume, ISME J., 6, 2269–2279, https://doi.org/10.1038/ismej.2012.64, 2012.

Baker, E. T., Walker, S. L., Massoth, G. J., and Resing, J. A.: The NE Lau Basin: Widespread and Abundant Hydrothermal Venting in the Back-Arc Region Behind a Superfast Subduction Zone, Front. Mar. Sci., 6, 382, https://doi.org/10.3389/fmars.2019.00382, 2019.

Beatty, J. T., Overmann, J., Lince, M. T., Manske, A. K., Lang, A. S., Blankenship, R. E., Van Dover, C. L., Martinson, T. A., and Plumley, F. G.: An obligately photosynthetic bacterial anaerobe from a deep-sea hydrothermal vent, P. Natl. Acad. Sci. USA, 102, 9306–9310, https://doi.org/10.1073/pnas.0503674102, 2005.

Beaulieu, S. E., Baker, E. T., German, C. R., and Maffei, A.: An authoritative global database for active submarine hydrothermal vent fields, Geochem. Geophy. Geosy., 14, 4892–4905, https://doi.org/10.1002/2013GC004998, 2013.

Behrenfeld, M. J., Worthington, K., Sherrell, R. M., Chavez, F. P., Strutton, P., McPhaden, M., and Shea, D. M.: Controls on tropical Pacific Ocean productivity revealed through nutrient stress diagnostics, Nature, 442, 1025–1028, 2006.

Bennett, S. A., Achterberg, E. P., Connelly, D. P., Statham, P. J., Fones, G. R., and German, C. R.: The distribution and stabilisation of dissolved Fe in deep-sea hydrothermal plumes, Earth Planet. Sc. Lett., 270, 157–167, https://doi.org/10.1016/j.epsl.2008.01.048, 2008.

Bennett, S. A., Coleman, M., Huber, J. A., Reddington, E., Kinsey, J. C., McIntyre, C., Seewald, J. S., and German, C. R.: Trophic regions of a hydrothermal plume dispersing away from an ultramafic-hosted vent-system: Von Damm vent-site, Mid-Cayman Rise, Geochem. Geophy. Geosy., 14, 317–327, https://doi.org/10.1002/ggge.20063, 2013.

Bergauer, K., Fernandez-Guerra, A., Garcia, J. A. L., Sprenger, R. R., Stepanauskas, R., Pachiadaki, M. G., Jensen, O. N., and Herndl, G. J.: Organic matter processing by microbial communities throughout the Atlantic water column as revealed by metaproteomics, P. Natl. Acad. Sci. USA, 115, E400–E408, https://doi.org/10.1073/pnas.1708779115, 2018.

Bertrand, E. M., McCrow, J. P., Moustafa, A., Zheng, H., McQuaid, J. B., Delmont, T. O., Post, A. F., Sipler, R. E., Spackeen, J. L., Xu, K., Bronk, D. A., Hutchins, D. A., and Allen, A. E.: Phytoplankton-bacterial interactions mediate micronutrient colimitation at the coastal Antarctic sea ice edge, P. Natl. Acad. Sci. USA, 112, 9938–43, https://doi.org/10.1073/pnas.1501615112, 2015.

Biller, D. V. and Bruland, K. W.: Analysis of Mn, Fe, Co, Ni, Cu, Zn, Cd, and Pb in seawater using the Nobias-chelate PA1 resin and magnetic sector inductively coupled plasma mass spectrometry (ICP-MS), Mar. Chem., 130/131, 12–20, https://doi.org/10.1016/j.marchem.2011.12.001, 2012.

Bostock, H. C., Opdyke, B. N., and Williams, M. J. M.: Characterising the intermediate depth waters of the Pacific Ocean using δ^{13}C and other geochemical tracers, Deep-Sea Res. Pt. I, 57, 847–859, https://doi.org/10.1016/j.dsr.2010.04.005, 2010.

Bown, J., Laan, P., Ossebaar, S., Bakker, K., Rozema, P., and de Baar, H. J. W.: Bioactive trace metal time series during Austral summer in Ryder Bay, Western Antarctic Peninsula, Deep-Sea Res. Pt. II, 139, 103–119, https://doi.org/10.1016/j.dsr2.2016.07.004, 2017.

Boyle, E. A., Bergquist, B. A., Kayser, R. A., and Mahowald, N.: Iron, manganese, and lead at Hawaii Ocean Time-series station ALOHA: Temporal variability and an intermediate water hydrothermal plume, Geochim. Cosmochim. Ac., 69, 933–952, https://doi.org/10.1016/j.gca.2004.07.034, 2005.

Brooks, J. P., Edwards, D. J., Harwich Jr., M. D., Rivera, M. D., Fettweis, J. M., Serrano, M. G., Reris, R. A., Sheth, N. U., Huang, B., Girerd, P., Vaginal Microbiome Consortium, Strauss III, J. F., Jefferson, K. K., and Buck, G. A.: The truth about metagenomics: quantifying and counteracting bias in 16S rRNA studies, BMC Microbiol., 15, 66, https://doi.org/10.1186/s12866-015-0351-6, 2015.

Bruland, K. W. and Lohan, M. C.: Controls of Trace Metals in Seawater, in: Treatise on Geochemistry, Vol. 6, 23–47, 2003.

Chang, C., Xu, K., Guo, C., Wang, J., Yan, Q., Zhang, J., He, F., and Zhu, Y.: PANDA-view: An easy-to-use tool for statistical analysis and visualization of quantitative proteomics data, Bioinformatics, 34, 3594–3596, https://doi.org/10.1093/bioinformatics/bty408, 2018.

Chen, Y., Wei, D., Wang, Y., and Zhang, X.: The role of interactions between bacterial chaperone, aspartate aminotransferase, and viral protein during virus infection in high temperature environment: The interactions between bacterium and virus proteins, BMC Microbiol., 13, 48, https://doi.org/10.1186/1471-2180-13-48, 2013.

Cohen, N. R., Moran, D. M., McIlvin, M. R., McCrow, J. P., Allen, A. E., and Saito, M. A.: Metzyme metaproteomic data set on PRIDE (3–51 µm filter fraction), Proteome Xchange [data set], https://doi.org/10.6019/PXD014230, 2020.

Cohen, N. R., McIlvin, M. R., Moran, D. M., Held, N. A., Saunders, J. K., Hawco, N. J., Brosnahan, M., DiTullio, G. R., Lamborg, C., McCrow, J. P., Dupont, C. L., Allen, A. E., and Saito, M. A.: Dinoflagellates alter their carbon and nutrient metabolic strategies across environmental gradients in the central Pacific Ocean, Nat. Microbiol., 6, 173–186, https://doi.org/10.1038/s41564-020-00814-7, 2021a.

Cohen, N. R., Moran, D. M., McIlvin, M. R., Hawco, N. J., Lamborg, C. H., and Saito, M. A.: Biological and Chemical Oceanography Data Repository – Metzyme dissolved trace metals and metadata, BCO-DMO [data set], available at: https://www.bco-dmo.org/dataset/836347, last access: 25 September 2021b.

Cowen, J. P. and Bruland, K. W.: Metal deposits associated with bacteria: implications for Fe and Mn marine biogeochemistry, Deep-Sea Res. Pt. A, 32, 253–272, https://doi.org/10.1016/0198-0149(85)90078-0, 1985.

Cowen, J. P., Massoth, G. J., and Feely, R. A.: Scavenging rates of dissolved manganese in a hydrothermal vent plume, Deep-Sea Res. Pt. A, 37, 1619–1637, https://doi.org/10.1016/0198-0149(90)90065-4, 1990.

Cullen, J. T.: On the nonlinear relationship between dissolved cadmium and phosphate in the modern global ocean: Could chronic iron limitation of phytoplankton growth cause the kink?, Limnol. Oceanogr., 51, 1369–1380, https://doi.org/10.4319/lo.2006.51.3.1369, 2006.

Dick, G. J.: The microbiomes of deep-sea hydrothermal vents: distributed globally, shaped locally, Nat. Rev. Microbiol., 17, 271–283, https://doi.org/10.1038/s41579-019-0160-2, 2019.

Dick, G. J., Lee, Y. E., and Tebo, B. M.: Manganese(II)-oxidizing Bacillus spores in Guaymas basin hydrothermal sediments and plumes, Appl. Environ. Microbiol., 72, 3184–3190, https://doi.org/10.1128/AEM.72.5.3184-3190.2006, 2006.

Dick, G. J., Anantharaman, K., Baker, B. J., Li, M., Reed, D. C., and Sheik, C. S.: The microbiology of deep-sea hydrothermal vent plumes: Ecological and biogeographic linkages to seafloor and water column habitats, Front. Microbiol., 4, 124, https://doi.org/10.3389/fmicb.2013.00124, 2013.

Diemer, J., Quétel, C. R., and Taylor, P. D. P.: Comparison of the performance of different ICP-MS instruments on the measurement of Cu in a water sample by ICP-IDMS, J. Anal. Atom. Spectr., 17, 1137–1142, 2002.

Djurhuus, A., Mikalsen, S. O., Giebel, H. A., and Rogers, A. D.: Cutting through the smoke: The diversity of microorganisms in deep-sea hydrothermal plumes, R. Soc. Open Sci., 4, 160829, https://doi.org/10.1098/rsos.160829, 2017.

Edgcomb, V. P., Molyneaux, S. J., Saito, M. A., Lloyd, K., Böer, S., Wirsen, C. O., Atkins, M. S., and Teske, A.: Sulfide Ameliorates Metal Toxicity for Deep-Sea Hydrothermal Vent Archaea, Appl. Environ. Microbiol., 70, 2551–2555, https://doi.org/10.1128/AEM.70.4.2551-2555.2004, 2004.

Fitzsimmons, J. N., Boyle, E. A., and Jenkins, W. J.: Distal transport of dissolved hydrothermal iron in the deep South Pacific Ocean, P. Natl. Acad. Sci. USA, 111, 16654, https://doi.org/10.1073/pnas.1418778111, 2014.

Fitzsimmons, J. N., John, S. G., Marsay, C. M., Hoffman, C. L., Nicholas, S. L., Toner, B. M., German, C. R., and Sherrell, R. M.: Iron persistence in a distal hydrothermal plume supported by dissolved-particulate exchange, Nat. Geosci., 10, 195–201, https://doi.org/10.1038/ngeo2900, 2017.

Frew, R. D. and Hunter, K. A.: Cadmium-phosphorus cycling at the subtropical convergence south of New Zealand, Mar. Chem., 51, 223–237, https://doi.org/10.1016/0304-4203(95)00057-7, 1995.

Fuchida, S., Mizuno, Y., Masuda, H., Toki, T., and Makita, H.: Concentrations and distributions of amino acids in black and white smoker fluids at temperatures over 200 °C, Org. Geochem., 66, 98–106, https://doi.org/10.1016/j.orggeochem.2013.11.008, 2014.

Garber, A. I., Nealson, K. H., Okamoto, A., McAllister, S. M., Chan, C. S., Barco, R. A., and Merino, N.: FeGenie: A Comprehensive Tool for the Identification of Iron Genes and Iron Gene Neighborhoods in Genome and Metagenome Assemblies, Front. Microbiol., 11, 37, https://doi.org/10.3389/fmicb.2020.00037, 2020.

Gartman, A. and Findlay, A. J.: Impacts of hydrothermal plume processes on oceanic metal cycles and transport, Nat. Geosci., 13, 396–402, https://doi.org/10.1038/s41561-020-0579-0, 2020.

German, C. R. and Seyfried, W. E.: Hydrothermal Processes, in: Treatise on Geochemistry, 2nd Edn., Vol. 8, 191–233, 2013.

German, C. R., Baker, E. T., Connelly, D. P., Lupton, J. E., Resing, J., Prien, R. D., Walker, S. L., Edmonds, H. N., and Langmuir, C. H.: Hydrothermal exploration of the Fonualei Rift and Spreading Center and the Northeast Lau Spreading Center, Geochem. Geophy. Geosy., 7, Q11022, https://doi.org/10.1029/2006GC001324, 2006.

Glover, D. M., Jenkins, W. J., Doney, S. C., Glover, D. M., Jenkins, W. J., and Doney, S. C.: Least squares and regression techniques, goodness of fit and tests, and nonlinear least squares techniques, in: Modeling Methods for Marine Science, 49–74, Cambridge University Press, Cambridge, https://doi.org/10.1017/CBO9780511975721.004, 2012.

Goepfert, T. J.: Urea and nickel utilization in marine cyanobacteria as evaluated by incubation, proteomic, and uptake techniques, available at: https://dspace.mit.edu/handle/1721.1/82303 (last access: 26 September 2021), 2013.

Guillou, L., Bachar, D., Audic, S., Bass, D., Berney, C., Bittner, L., Boutte, C., Burgaud, G., De Vargas, C., Decelle, J., Del Campo, J., Dolan, J. R., Dunthorn, M., Edvardsen, B., Holzmann, M., Kooistra, W. H. C. F., Lara, E., Le Bescot, N., Logares, R., Mahé, F., Massana, R., Montresor, M., Morard, R., Not, F., Pawlowski, J., Probert, I., Sauvadet, A. L., Siano, R., Stoeck, T., Vaulot, D., Zimmermann, P., and Christen, R.: The Protist Ribosomal Reference database (PR2): A catalog of unicellular eukaryote Small Sub-Unit rRNA sequences with curated taxonomy, Nucleic Acids Res., 41, D597–D604, https://doi.org/10.1093/nar/gks1160, 2013.

Haalboom, S., M. Price, D., Mienis, F., D. L. Van Bleijswijk, J., C. De Stigter, H., J. Witte, H., Reichart, G. J., and C. A. Duineveld, G.: Patterns of (trace) metals and microorganisms in the Rainbow hydrothermal vent plume at the Mid-Atlantic Ridge, Biogeosciences, 17, 2499–2519, https://doi.org/10.5194/bg-17-2499-2020, 2020.

Hawco, N. J., McIlvin, M. M., Bundy, R. M., Tagliabue, A., Goepfert, T. J., Moran, D. M., Valentin-Alvarado, L., DiTullio, G. R., and Saito, M. A.: Minimal cobalt metabolism in the marine cyanobacterium *Prochlorococcus*, P. Natl. Acad. Sci. USA, 117, 15740, https://doi.org/10.1073/pnas.2001393117, 2020.

Hawkes, J. A., Connelly, D. P., Gledhill, M., and Achterberg, E. P.: The stabilisation and transportation of dissolved iron from high temperature hydrothermal vent systems, Earth Planet. Sc. Lett., 375, 280–290, https://doi.org/10.1016/j.epsl.2013.05.047, 2013.

Hawkins, J.: "Black smoker" vent chimneys, Eos, Trans. Am. Geophys. Union, 67, 430, https://doi.org/10.1029/eo067i017p00430-01, 1986.

Herzig, P. M., Hannington, M. D., Fouquet, Y., Von Stackelberg, U., and Petersen, S.: Gold-rich polymetallic sulfides from the lau back arc and implications for the geochemistry of gold in sea-floor hydrothermal systems of the Southwest Pacific, Econ. Geol., 88, 2182–2209, https://doi.org/10.2113/gsecongeo.88.8.2182, 1993.

Horner, T. J., Williams, H. M., Hein, J. R., Saito, M. A., Burton, K. W., Halliday, A. N., and Nielsen, S. G.: Persistence of deeply sourced iron in the Pacific Ocean, P. Natl. Acad. Sci. USA, 112, 1292–1297, https://doi.org/10.1073/pnas.1420188112, 2015.

Hsu-Kim, H., Mullaugh, K. M., Tsang, J. J., Yucel, M., and Luther, G. W.: Formation of Zn- and Fe-sulfides near hydrothermal vents at the Eastern Lau Spreading Center: Implications for sulfide bioavailability to chemoautotrophs, Geochem. Trans., 9, 6, https://doi.org/10.1186/1467-4866-9-6, 2008.

Hu, S. K., Herrera, E. L., Smith, A. R., Pachiadaki, M. G., Edgcomb, V. P., Sylva, S. P., Chan, E. W., Seewald, J. S., German, C. R., and Huber, J. A.: Protistan grazing impacts microbial communities and carbon cycling at deep-sea hydrothermal vents, P. Natl. Acad. Sci. USA, 118, e2102674118, https://doi.org/10.1073/pnas.2102674118, 2021.

Huber, J. A., Mark Welch, D. B., Morrison, H. G., Huse, S. M., Neal, P. R., Butterfield, D. A., and Sogin, M. L.: Microbial population structures in the deep marine biosphere, Science, 318, 97–100, https://doi.org/10.1126/science.1146689, 2007.

Jackson, S. L., Spence, J., Janssen, D. J., Ross, A. R. S., and Cullen, J. T.: Determination of Mn, Fe, Ni, Cu, Zn, Cd and Pb in seawater using offline extraction and triple quadrupole ICP-MS/MS, J. Anal. At. Spectrom., 33, 304–313, https://doi.org/10.1039/C7JA00237H, 2018.

Jeanthon, C.: Molecular ecology of hydrothermal vent microbial communities, Antonie van Leeuwenhoek, Int. J. Gen. Mol. Microbiol., 77, 117–133, https://doi.org/10.1023/A:1002463825025, 2000.

Jenkins, W. J., Doney, S. C., Fendrock, M., Fine, R., Gamo, T., Jean-Baptiste, P., Key, R., Klein, B., Lupton, J. E., Newton, R., Rhein, M., Roether, W., Sano, Y., Schlitzer, R., Schlosser, P., and Swift, J.: A comprehensive global oceanic dataset of helium isotope and tritium measurements, Earth Syst. Sci. Data, 11, 441–454, https://doi.org/10.5194/essd-11-441-2019, 2019a.

Jenkins, W. J., Lott, D. E., and Cahill, K. L.: A determination of atmospheric helium, neon, argon, krypton, and xenon solubility concentrations in water and seawater, Mar. Chem., 211, 94–107, https://doi.org/10.1016/j.marchem.2019.03.007, 2019b.

Jenkins, W. J., Hatta, M., Fitzsimmons, J. N., Schlitzer, R., Lanning, N. T., Shiller, A., Buckley, N. R., German, C. R., Lott, D. E., Weiss, G., Whitmore, L., Casciotti, K., Lam, P. J., Cutter, G. A., and Cahill, K. L.: An intermediate-depth source of hydrothermal ^{3}He and dissolved iron in the North Pacific, Earth Planet. Sc. Lett., 539, 116223, https://doi.org/10.1016/j.epsl.2020.116223, 2020.

Jickells, T. D., An, Z. S., Andersen, K. K., Baker, A. R., Bergametti, C., Brooks, N., Cao, J. J., Boyd, P. W., Duce, R. A., Hunter, K. A., Kawahata, H., Kubilay, N., LaRoche, J., Liss, P. S., Mahowald, N., Prospero, J. M., Ridgwell, A. J., Tegen, I., and Torres, R.: Global iron connections between desert dust, ocean biogeochemistry, and climate, Science, 308, 67–71, https://doi.org/10.1126/science.1105959, 2005.

John, S. G., Helgoe, J., and Townsend, E.: Biogeochemical cycling of Zn and Cd and their stable isotopes in the Eastern Tropical South Pacific, Mar. Chem., 201, 256–262, https://doi.org/10.1016/j.marchem.2017.06.001, 2018.

Kim, J., Son, S. K., Son, J. W., Kim, K. H., Shim, W. J., Kim, C. H., and Lee, K. Y.: Venting sites along the Fonualei and Northeast Lau Spreading Centers and evidence of hydrothermal activity at an off-axis caldera in the northeastern Lau Basin, Geochem. J., 43, 1–13, https://doi.org/10.2343/geochemj.0.0164, 2009.

Kirchman, D. L.: Microbial proteins for organic material degradation in the deep ocean, P. Natl. Acad. Sci. USA, 115, 445–447, https://doi.org/10.1073/pnas.1720765115, 2018.

Kogut, M. B. and Voelker, B. M.: Kinetically inert Cu in coastal waters, Environ. Sci. Technol., 37, 509–518, https://doi.org/10.1021/es020723d, 2003.

Lane, E. S., Jang, K., Cullen, J. T., and Maldonado, M. T.: The interaction between inorganic iron and cadmium uptake in the marine diatom Thalassiosira oceanica, Limnol. Oceanogr., 53, 1784–1789, https://doi.org/10.4319/lo.2008.53.5.1784, 2008.

Li, J., Yang, J., Sun, M., Su, L., Wang, H., Gao, J., and Bai, S.: Distribution and Succession of Microbial Communities Along the Dispersal Pathway of Hydrothermal Plumes on the Southwest Indian Ridge, Front. Mar. Sci., 7, 940, https://doi.org/10.3389/fmars.2020.581381, 2020.

Li, M., Toner, B. M., Baker, B. J., Breier, J. A., Sheik, C. S., and Dick, G. J.: Microbial iron uptake as a mechanism for dispersing iron from deep-sea hydrothermal vents, Nat. Commun., 5, 3192, https://doi.org/10.1038/ncomms4192, 2014.

Little, S. H., Archer, C., Milne, A., Schlosser, C., Achterberg, E. P., Lohan, M. C., and Vance, D.: Paired dissolved and particulate phase Cu isotope distributions in the South Atlantic, Chem. Geol., 502, 29–43, https://doi.org/10.1016/j.chemgeo.2018.07.022, 2018.

Lupton, J. E., Pyle, D. G., Jenkins, W. J., Greene, R., and Evans, L.: Evidence for an extensive hydrothermal plume in the Tonga-Fiji region of the South Pacific, Geochem. Geophy. Geosy., 5, Q01003, https://doi.org/10.1029/2003GC000607, 2004.

Lupton, J. E., Arculus, R. J., Evans, L. J., and Graham, D. W.: Mantle hotspot neon in basalts from the Northwest Lau Back-arc Basin, Geophys. Res. Lett., 39, L08308, https://doi.org/10.1029/2012GL051201, 2012.

Lusty, P. A. J. and Murton, B. J.: Deep-ocean mineral deposits: Metal resources and windows into earth processes, Elements, 14, 301–306, https://doi.org/10.2138/gselements.14.5.301, 2018.

Marchitto, T. M., Curry, W. B., and Oppo, D. W.: Zinc concentrations in benthic foraminifera reflect seawater chemistry, Paleoceanography, 15, 299–306, https://doi.org/10.1029/1999PA000420, 2000.

Mars Brisbin, M., Conover, A. E., and Mitarai, S.: Influence of Regional Oceanography and Hydrothermal Activity on Protist Diversity and Community Structure in the Okinawa Trough, Microb. Ecol., 80, 746–761, https://doi.org/10.1007/s00248-020-01583-w, 2020.

Martinez, F., Taylor, B., Baker, E. T., Resing, J. A., and Walker, S. L.: Opposing trends in crustal thickness and spreading rate along the back-arc Eastern Lau Spreading Center: Implications for controls on ridge morphology, faulting, and hydrothermal activity, Earth Planet. Sc. Lett., 245, 655–672, https://doi.org/10.1016/j.epsl.2006.03.049, 2006.

McIlvin, M. R. and Saito, M. A.: Online Nanoflow Two-Dimension Comprehensive Active Modulation Reversed Phase–Reversed Phase Liquid Chromatography High-Resolution Mass Spectrometry for Metaproteomics of Environmental and Microbiome Samples, J. Proteome Res., 20, 4589–4597, https://doi.org/10.1021/acs.jproteome.1c00588, 2021.

McMurdie, P. J. and Holmes, S.: Phyloseq: An R Package for Reproducible Interactive Analysis and Graphics of Microbiome Census Data, PLoS One, 8, e61217, https://doi.org/10.1371/journal.pone.0061217, 2013.

Merino, N., Aronson, H. S., Bojanova, D. P., Feyhl-Buska, J., Wong, M. L., Zhang, S., and Giovannelli, D.: Living at the extremes: Extremophiles and the limits of life in a planetary context, Front. Microbiol., 10, 780, https://doi.org/10.3389/fmicb.2019.00780, 2019.

Middag, R., van Heuven, S. M. A. C., Bruland, K. W., and de Baar, H. J. W.: The relationship between cadmium and phosphate in the Atlantic Ocean unravelled, Earth Planet. Sc. Lett., 492, 79–88, https://doi.org/10.1016/j.epsl.2018.03.046, 2018.

Middag, R., de Baar, H. J. W., and Bruland, K. W.: The Relationships Between Dissolved Zinc and Major Nutrients Phosphate and Silicate Along the GEOTRACES GA02 Transect in the West Atlantic Ocean, Global Biogeochem. Cy., 33, 63–84, https://doi.org/10.1029/2018GB006034, 2019.

Milne, A., Landing, W., Bizimis, M., and Morton, P.: Determination of Mn, Fe, Co, Ni, Cu, Zn, Cd and Pb in seawater using high resolution magnetic sector inductively coupled mass spectrometry (HR-ICP-MS), Anal. Chim. Acta, 665, 200–207, 2010.

Mino, S., Maikita, H., Toki, T., Miyazaki, J., Kato, S., Watanabe, H., Imachi, H., Watsuji, T., Nunoura, T., Kojima, S., Sawabe, T., Takai, K., and Nakagawa, S.: Biogeography of Persephonella in deep-sea hydrothermal vents of the Western Pacific, Front. Microbiol., 4, 107, https://doi.org/10.3389/fmicb.2013.00107, 2013.

Mino, S., Nakagawa, S., Makita, H., Toki, T., Miyazaki, J., Sievert, S. M., Polz, M. F., Inagaki, F., Godfroy, A., Kato, S., Watanabe, H., Nunoura, T., Nakamura, K., Imachi, H., Watsuji, T., Kojima, S., Takai, K., and Sawabe, T.: Endemicity of the cosmopolitan mesophilic chemolithoautotropH Sulfurimonas at deep-sea hydrothermal vents, ISME J., 11, 909–919, https://doi.org/10.1038/ismej.2016.178, 2017.

Moffett, J. W. and Ho, J.: Oxidation of cobalt and manganese in seawater via a common microbially catalyzed pathway, Geochim.

Cosmochim. Ac., 60, 3415–3424, https://doi.org/10.1016/0016-7037(96)00176-7, 1996.

Moore, C. M., Mills, M. M., Arrigo, K. R., Berman-Frank, I., Bopp, L., Boyd, P. W., Galbraith, E. D., Geider, R. J., Guieu, C., Jaccard, S. L., Jickells, T. D., La Roche, J., Lenton, T. M., Mahowald, N. M., Marañón, E., Marinov, I., Moore, J. K., Nakatsuka, T., Oschlies, A., Saito, M. A., Thingstad, T. F., Tsuda, A., and Ulloa, O.: Processes and patterns of oceanic nutrient limitation, Nat. Geosci., 6, 701–710, https://doi.org/10.1038/ngeo1765, 2013.

Moore, J. K., Doney, S. C., Glover, D. M., and Fung, I. Y.: Iron cycling and nutrient-limitation patterns in surface waters of the World Ocean, Deep-Sea Res. Pt. II, 49, 463–507, 2001.

Munson, K. M., Lamborg, C. H., Swarr, G. J., and Saito, M. A.: Mercury species concentrations and fluxes in the Central Tropical Pacific Ocean, Global Biogeochem. Cy., 29, 656–676, https://doi.org/10.1002/2015GB005120, 2015.

Murdock, S. A. and Juniper, S. K.: Hydrothermal vent protistan distribution along the Mariana arc suggests vent endemics may be rare and novel, Environ. Microbiol., 21, 3796–3815, https://doi.org/10.1111/1462-2920.14729, 2019.

Muthusamy, S., Baltar, F., González, J. M., and Pinhassi, J.: Dynamics of metabolic activities and gene expression in the Roseobacter clade bacterium *Phaeobacter* sp. strain MED193 during growth with thiosulfate, Appl. Environ. Microbiol., 80, 6933–6942, https://doi.org/10.1128/AEM.02038-14, 2014.

Ndung'u, K., Franks, R. P., Bruland, K. W., and Flegal, A. R.: Organic complexation and total dissolved trace metal analysis in estuarine waters: Comparison of solvent-extraction graphite furnace atomic absorption spectrometric and chelating resin flow injection inductively coupled plasma-mass spectrometric analysis, Anal. Chim. Acta, 481, 127–138, 2003.

Noinaj, N., Guillier, M., Barnard, T. J., and Buchanan, S. K.: TonB-Dependent Transporters: Regulation, Structure, and Function, Annu. Rev. Microbiol., 64, 43–60, https://doi.org/10.1146/annurev.micro.112408.134247, 2010.

Olsen, B. R., Troedsson, C., Hadziavdic, K., Pedersen, R.-B., and Rapp, H. T.: The influence of vent systems on pelagic eukaryotic micro-organism composition in the Nordic Seas, Polar Biol., 38, 547–558, https://doi.org/10.1007/s00300-014-1621-8, 2015.

Orellana, L. H., Hatt, J. K., Iyer, R., Chourey, K., Hettich, R. L., Spain, J. C., Yang, W. H., Chee-Sanford, J. C., Sanford, R. A., Löffler, F. E., and Konstantinidis, K. T.: Comparing DNA, RNA and protein levels for measuring microbial dynamics in soil microcosms amended with nitrogen fertilizer, Sci. Rep., 9, 17630, https://doi.org/10.1038/s41598-019-53679-0, 2019.

Pachiadaki, M. G., Sintes, E., Bergauer, K., Brown, J. M., Record, N. R., Swan, B. K., Mathyer, M. E., Hallam, S. J., Lopez-Garcia, P., Takaki, Y., Nunoura, T., Woyke, T., Herndl, G. J., and Stepanauskas, R.: Major role of nitrite-oxidizing bacteria in dark ocean carbon fixation, Science, 358, 1046–1051, https://doi.org/10.1126/science.aan8260, 2017.

Podell, S. and Gaasterland, T.: DarkHorse: A method for genome-wide prediction of horizontal gene transfer, Genome Biol., 8, R16, https://doi.org/10.1186/gb-2007-8-2-r16, 2007.

Posacka, A. M., Semeniuk, D. M., Whitby, H., van den Berg, C. M. G., Cullen, J. T., Orians, K., and Maldonado, M. T.: Dissolved copper (dCu) biogeochemical cycling in the subarctic Northeast

Pacific and a call for improving methodologies, Mar. Chem., 196, 47–61, https://doi.org/10.1016/j.marchem.2017.05.007, 2017.

Quast, C., Pruesse, E., Yilmaz, P., Gerken, J., Schweer, T., Yarza, P., Peplies, J., and Glöckner, F. O.: The SILVA ribosomal RNA gene database project: Improved data processing and web-based tools, Nucleic Acids Res., 41, D590–D596, https://doi.org/10.1093/nar/gks1219, 2013.

Quéroué, F., Townsend, A., Van Der Merwe, P., Lannuzel, D., Sarthou, G., Bucciarelli, E., and Bowie, A.: Advances in the offline trace metal extraction of Mn, Co, Ni, Cu, Cd, and Pb from open ocean seawater samples with determination by sector field ICP-MS analysis, Anal. Methods, 6, 2837–2847, https://doi.org/10.1039/c3ay41312h, 2014.

Rapp, I., Schlosser, C., Rusiecka, D., Gledhill, M., and Achterberg, E. P.: Automated preconcentration of Fe, Zn, Cu, Ni, Cd, Pb, Co, and Mn in seawater with analysis using high-resolution sector field inductively-coupled plasma mass spectrometry, Anal. Chim. Acta, 976, 1–13, https://doi.org/10.1016/j.aca.2017.05.008, 2017.

Reed, D. C., Breier, J. A., Jiang, H., Anantharaman, K., Klausmeier, C. A., Toner, B. M., Hancock, C., Speer, K., Thurnherr, A. M., and Dick, G. J.: Predicting the response of the deep-ocean microbiome to geochemical perturbations by hydrothermal vents, ISME J., 9, 1857–1869, https://doi.org/10.1038/ismej.2015.4, 2015.

Reid, J. L.: On the total geostrophic circulation of the Pacific Ocean: Flow patterns, tracers, and transports, Prog. Oceanogr., 39, 263–352, https://doi.org/10.1016/S0079-6611(97)00012-8, 1997.

Resing, J. A., Sedwick, P. N., German, C. R., Jenkins, W. J., Moffett, J. W., Sohst, B. M., and Tagliabue, A.: Basin-scale transport of hydrothermal dissolved metals across the South Pacific Ocean, Nature, 523, 200–203, https://doi.org/10.1038/nature14577, 2015.

Reveillaud, J., Reddington, E., McDermott, J., Algar, C., Meyer, J. L., Sylva, S., Seewald, J., German, C. R., and Huber, J. A.: Subseafloor microbial communities in hydrogen-rich vent fluids from hydrothermal systems along the Mid-Cayman Rise, Environ. Microbiol., 18, 1970–1987, https://doi.org/10.1111/1462-2920.13173, 2016.

Rodionov, D. A., Hebbeln, P., Gelfand, M. S., and Eitinger, T.: Comparative and functional genomic analysis of prokaryotic nickel and cobalt uptake transporters: Evidence for a novel group of ATP-binding cassette transporters, J. Bacteriol., 188, 317–327, https://doi.org/10.1128/JB.188.1.317-327.2006, 2006.

Roshan, S., Wu, J., and Jenkins, W. J.: Long-range transport of hydrothermal dissolved Zn in the tropical South Pacific, Mar. Chem., 183, 25–32, https://doi.org/10.1016/j.marchem.2016.05.005, 2016.

Roshan, S., Wu, J., and DeVries, T.: Controls on the Cadmium-Phosphate Relationship in the Tropical South Pacific, Global Biogeochem. Cy., 31, 1516–1527, https://doi.org/10.1002/2016GB005556, 2017.

Rudnicki, M. D. and German, C. R.: Temporal variability of the hydrothermal plume above the Kairei vent field, 25° S, Central Indian Ridge, Geochem. Geophy. Geosy., 3, 2, https://doi.org/10.1029/2001gc000240, 2002.

Saito, M. A. and Moffett, J. W.: Complexation of cobalt by natural organic ligands in the Sargasso sea as determined by a new high-

sensitivity electrochemical cobalt speciation method suitable for open ocean work, Mar. Chem., 75, 49–68, 2001.

Saito, M. and Lamborg, C.: Connecting Trace Elements and Metalloenzymes Across Marine Biogeochemical Gradients, BCO-DMO [data set], available at: https://www.bco-dmo.org/project/2236, last access: 25 September 2021.

Saito, M. A., Goepfert, T. J., Noble, A. E., Bertrand, E. M., Sedwick, P. N., and Ditullio, G. R.: A seasonal study of dissolved cobalt in the Ross Sea, Antarctica: Micronutrient behavior, absence of scavenging, and relationships with Zn, Cd, and P, Biogeosciences, 7, 4059–4082, https://doi.org/10.5194/bg-7-4059-2010, 2010.

Saito, M. A., Noble, A. E., Tagliabue, A., Goepfert, T. J., Lamborg, C. H., and Jenkins, W. J.: Slow-spreading submarine ridges in the South Atlantic as a significant oceanic iron source, Nat. Geosci., 6, 775–779, https://doi.org/10.1038/ngeo1893, 2013.

Saito, M. A., McIlvin, M. R., Moran, D. M., Goepfert, T. J., DiTullio, G. R., Post, A. F., and Lamborg, C. H.: Multiple nutrient stresses at intersecting Pacific Ocean biomes detected by protein biomarkers, Science, 345, 1173–1177, https://doi.org/10.1126/science.1256450, 2014.

Saito, M. A., Dorsk, A., Anton, F., Mcilvin, M. R., Rapp, M. S., Ditullio, G. R., and Moran, D. M.: Needles in the blue sea: Subspecies specificity in targeted protein biomarker analyses within the vast oceanic microbial metaproteome, Proteomics, 15, 3521–3531, https://doi.org/10.1002/pmic.201400630, 2015.

Saito, M. A., Noble, A. E., Hawco, N., Twining, B. S., Ohnemus, D. C., John, S. G., Lam, P., Conway, T. M., Johnson, R., Moran, D., and McIlvin, M.: The acceleration of dissolved cobalt's ecological stoichiometry due to biological uptake, remineralization, and scavenging in the Atlantic Ocean, Biogeosciences, 14, 4637–4662, https://doi.org/10.5194/bg-14-4637-2017, 2017.

Saito, M. A., McIlvin, M. R., Moran, D. M., Santoro, A. E., Dupont, C. L., Rafter, P. A., Saunders, J. K., Kaul, D., Lamborg, C. H., Westley, M., Valois, F., and Waterbury, J. B.: Abundant nitrite-oxidizing metalloenzymes in the mesopelagic zone of the tropical Pacific Ocean, Nat. Geosci., 13, 355–362, https://doi.org/10.1038/s41561-020-0565-6, 2020.

Santoro, A. E., Saito, M. A., Goepfert, T. J., Lamborg, C. H., Dupont, C. L., and DiTullio, G. R.: Thaumarchaeal ecotype distributions across the equatorial Pacific Ocean and their potential roles in nitrification and sinking flux attenuation, Limnol. Oceanogr., 62, 1984–2003, https://doi.org/10.1002/lno.10547, 2017.

Sheik, C. S., Anantharaman, K., Breier, J. A., Sylvan, J. B., Edwards, K. J., and Dick, G. J.: Spatially resolved sampling reveals dynamic microbial communities in rising hydrothermal plumes across a back-arc basin, ISME J., 9, 1434–1445, https://doi.org/10.1038/ismej.2014.228, 2015.

Sieber, M., Conway, T. M., de Souza, G. F., Obata, H., Takano, S., Sohrin, Y., and Vance, D.: Physical and biogeochemical controls on the distribution of dissolved cadmium and its isotopes in the Southwest Pacific Ocean, Chem. Geol., 511, 494–509, https://doi.org/10.1016/j.chemgeo.2018.07.021, 2019.

Sohrin, Y., Urushihara, S., Nakatsuka, S., Kono, T., Higo, E., Minami, T., Norisuye, K., and Umetani, S.: Multielemental determination of GEOTRACES key trace metals in seawater by ICPMS after preconcentration using an ethylenediamine-

triacetic acid chelating resin, Anal. Chem., 80, 6267–6273, https://doi.org/10.1021/ac800500f, 2008.

Speer, K. and Thurnherr, A. M.: The lau basin float experiment (LAUB-FLEX), Oceanography, 25, 284–285, https://doi.org/10.5670/oceanog.2012.27, 2012.

Staudigel, H., Hart, S. R., Koppers, A. A. P., Constable, C., Workman, R., Kurz, M., and Baker, E. T.: Hydrothermal venting at Vailulu'u Seamount: The smoking end of the Samoan chain, Geochem., Geophy. Geosy., 5, Q02003, https://doi.org/10.1029/2003GC000626, 2004.

Staudigel, H., Hart, S. R., Pile, A., Bailey, B. E., Baker, E. T., Brooke, S., Connelly, D. P., Haucke, L., German, C. R., Hudson, I., Jones, D., Koppers, A. A. P., Konter, J., Lee, R., Pietsch, T. W., Tebo, B. M., Templeton, A. S., Zierenberg, R., and Young, C. M.: Vailulu'u seamount, Samoa: Life and death on an active submarine volcano, P. Natl. Acad. Sci. USA, 103, 6448–6453, https://doi.org/10.1073/pnas.0600830103, 2006.

Sunda, W. G.: Feedback interactions between trace metal nutrients and phytoplankton in the ocean, Front. Microbiol., 3, 204, https://doi.org/10.3389/fmicb.2012.00204, 2012.

Sunda, W. G. and Huntsman, S. A.: Effect of Zn, Mn, and Fe on Cd accumulation in phytoplankton: Implications for oceanic Cd cycling, Limnol. Oceanogr., 45, 1501–1516, https://doi.org/10.4319/lo.2000.45.7.1501, 2000.

Sunda, W. G., Huntsman, S. A., and Harvey, G. R.: Photoreduction of manganese oxides in seawater and its geochemical and biological implications, Nature, 301, 234–236, https://doi.org/10.1038/301234a0, 1983.

Sylvan, J. B., Toner, B. M., and Edwards, K. J.: Life and death of deep-sea vents: Bacterial diversity and ecosystem succession on inactive hydrothermal sulfides, mBio, 3, 1–10, https://doi.org/10.1128/mBio.00279-11, 2012.

Tagliabue, A., Bopp, L., Dutay, J. C., Bowie, A. R., Chever, F., Jean-Baptiste, P., Bucciarelli, E., Lannuzel, D., Remenyi, T., Sarthou, G., Aumont, O., Gehlen, M., and Jeandel, C.: Hydrothermal contribution to the oceanic dissolved iron inventory, Nat. Geosci., 3, 252–256, https://doi.org/10.1038/ngeo818, 2010.

Takai, K., Nunoura, T., Ishibashi, J. I., Lupton, J., Suzuki, R., Hamasaki, H., Ueno, Y., Kawagucci, S., Gamo, T., Suzuki, Y., Hirayama, H., and Horikoshi, K.: Variability in the microbial communities and hydrothermal fluid chemistry at the newly discovered Mariner hydrothermal field, southern Lau Basin, J. Geophys. Res.-Biogeo., 113, G02031, https://doi.org/10.1029/2007JG000636, 2008.

Takano, S., Tanimizu, M., Hirata, T., Shin, K. C., Fukami, Y., Suzuki, K., and Sohrin, Y.: A simple and rapid method for isotopic analysis of nickel, copper, and zinc in seawater using chelating extraction and anion exchange, Anal. Chim. Acta, 967, 1–11, https://doi.org/10.1016/j.aca.2017.03.010, 2017.

Tebo, B. M., Johnson, H. A., McCarthy, J. K., and Templeton, A. S.: Geomicrobiology of manganese(II) oxidation, Trends Microbiol., 13, 421–428, https://doi.org/10.1016/j.tim.2005.07.009, 2005.

Templeton, A. S., Staudigel, H., and Tebo, B. M.: Diverse Mn(II)-oxidizing bacteria isolated from submarine basalts at Loihi seamount, Geomicrobiol. J., 22, 127–139, https://doi.org/10.1080/01490450590945951, 2005.

Tivey, M. K.: Generation of seafloor hydrothermal vent fluids and associated mineral deposits, Oceanography, 20, 50–65, https://doi.org/10.5670/oceanog.2007.80, 2007.

Toner, B. M., Fakra, S. C., Manganini, S. J., Santelli, C. M., Marcus, M. A., Moffett, J. W., Rouxel, O., German, C. R., and Edwards, K. J.: Preservation of iron(II) by carbon-rich matrices in a hydrothermal plume, Nat. Geosci., 2, 197–201, https://doi.org/10.1038/ngeo433, 2009.

Toner, B. M., German, C. R., Dick, G. J., and Breier, J. A.: Deciphering the Complex Chemistry of Deep-Ocean Particles Using Complementary Synchrotron X-ray Microscope and Microprobe Instruments, Acc. Chem. Res., 49, 128–137, https://doi.org/10.1021/acs.accounts.5b00282, 2016.

van Hulten, M., Middag, R., Dutay, J.-C., de Baar, H., Roy-Barman, M., Gehlen, M., Tagliabue, A., and Sterl, A.: Manganese in the west Atlantic Ocean in the context of the first global ocean circulation model of manganese, Biogeosciences, 14, 1123–1152, https://doi.org/10.5194/bg-14-1123-2017, 2017.

VerBerkmoes, N. C., Denef, V. J., Hettich, R. L., and Banfield, J. F.: Systems Biology: Functional analysis of natural microbial consortia using community proteomics, Nat. Rev. Microbiol., 7, 196–205, https://doi.org/10.1038/nrmicro2080, 2009.

Vizcaíno, J. A., Côté, R. G., Csordas, A., Dianes, J. A., Fabregat, A., Foster, J. M., Griss, J., Alpi, E., Birim, M., Contell, J., O'Kelly, G., Schoenegger, A., Ovelleiro, D., Pérez-Riverol, Y., Reisinger, F., Ríos, D., Wang, R., and Hermjakob, H.: The Proteomics Identifications (PRIDE) database and associated tools: Status in 2013, Nucleic Acids Res., 41, D1063–D1069, https://doi.org/10.1093/nar/gks1262, 2013.

Ward, D. E., Shockley, K. R., Chang, L. S., Levy, R. D., Michel, J. K., Conners, S. B., and Kelly, R. M.: Proteolysis in hyperthermophilic microorganisms, Archaea, 1, 63–74, https://doi.org/10.1155/2002/503191, 2002.

Wei, D. and Zhang, X.: Proteomic Analysis of Interactions between a Deep-Sea Thermophilic Bacteriophage and Its Host at High Temperature, J. Virol., 84, 2365–2373, https://doi.org/10.1128/jvi.02182-09, 2010.

White, S. N., Chave, A. D., Reynolds, G. T., and Van Dover, C. L.: Ambient light emission from hydrothermal vents on the Mid-Atlantic Ridge, Geophys. Res. Lett., 29, 34-1–34-4, https://doi.org/10.1029/2002GL014977, 2002.

Wilson, S. T., Hawco, N. J., Armbrust, E. V., Barone, B., Björkman, K. M., Boysen, A. K., Burgos, M., Burrell, T. J., Casey, J. R., DeLong, E. F., Dugenne, M., Dutkiewicz, S., Dyhrman, S. T., Ferrón, S., Follows, M. J., Foreman, R. K., Funkey, C. P., Harke, M. J., Henke, B. A., Hill, C. N., Hynes, A. M., Ingalls, A. E., Jahn, O., Kelly, R. L., Knapp, A. N., Letelier, R. M., Ribalet, F., Shimabukuro, E. M., Tabata, R. K. S., Turk-Kubo, K. A., White, A. E., Zehr, J. P., John, S., and Karl, D. M.: Kīlauea lava fuels phytoplankton bloom in the North Pacific Ocean, Science, 365, 1040–1044, https://doi.org/10.1126/science.aax4767, 2019.

Wu, J., Wells, M. L., and Rember, R.: Dissolved iron anomaly in the deep tropical-subtropical Pacific: Evidence for long-range transport of hydrothermal iron, Geochim. Cosmochim. Ac., 75, 460–468, https://doi.org/10.1016/j.gca.2010.10.024, 2011.

Wuttig, K., Townsend, A. T., van der Merwe, P., Gault-Ringold, M., Holmes, T., Schallenberg, C., Latour, P., Tonnard, M., Rijkenberg, M. J. A., Lannuzel, D., and Bowie, A. R.: Critical evaluation of a seaFAST system for the analysis of trace metals in marine samples, Talanta, 197, 653–668, https://doi.org/10.1016/j.talanta.2019.01.047, 2019.

Xie, R. C., Galer, S. J. G., Abouchami, W., Rijkenberg, M. J. A., De Jong, J., De Baar, H. J. W., and Andreae, M. O.: The cadmium-phosphate relationship in the western South Atlantic – The importance of mode and intermediate waters on the global systematics, Mar. Chem., 177, 110–123, https://doi.org/10.1016/j.marchem.2015.06.011, 2015.

Yu, H. and Leadbetter, J. R.: Bacterial chemolithoautotrophy via manganese oxidation, Nature, 583, 453–458, https://doi.org/10.1038/s41586-020-2468-5, 2020.